Concentration and source changes of HONO during the COVID-19 lockdown in Beijing

Yusheng Zhang[1], Feixue Zheng[1], Zemin Feng[1,2], Chaofan Lian[3,4], Weigang Wang[3,4*], Xiaolong Fan[1,5,6], Wei Ma[1], Zhuohui Lin[1], Chang Li[1], Gen Zhang[7], Chao Yan[8,9], Ying Zhang[1,9],Veli-Matti Kerminen[1,8] , Federico Bianch[1,8], Tuukka Petäjä[1,8], Juha Kangasluoma[1,8], and Markku Kulmala[1,8], Yongchun Liu[1*]

1. Aerosol and Haze Laboratory, Advanced Innovation Center for Soft Matter Science and Engineering, Beijing University of Chemical Technology, Beijing, 100029, China
2. College of Chemical Engineering, North China University of Science and Technology, Tangshan 063210, China
3. State Key Laboratory for Structural Chemistry of Unstable and Stable Species, Beijing National Laboratory for Molecular Sciences (BNLMS), CAS Research/Education Center for Excellence in Molecular Sciences, Institute of Chemistry, Chinese Academy of Sciences, Beijing 100190, China
4. University of Chinese Academy of Sciences, Beijing 100049, China
5. Center for Excellence in Regional Atmospheric Environment, Institute of Urban Environment, Chinese Academy of Sciences, Xiamen 361021, China
6. Fujian Key Laboratory of Atmospheric Ozone Pollution Prevention, Institute of Urban Environment, Chinese Academy of Sciences, Xiamen 361021, China
7. State Key Laboratory of Severe Weather & Key Laboratory of Atmospheric Chemistry of China Meteorological Administration (CMA), Chinese Academy of Meteorological Sciences (CAMS), Beijing 100081, China
8. Institute for Atmospheric and Earth System Research/Physics, Faculty of Science, University of Helsinki, P.O. Box 64, FI-00014, Finland
9. Joint International Research Laboratory of Atmospheric and Earth System Science, School of Atmospheric Sciences, Nanjing University, Nanjing, China.

*Correspondence: Yongchun Liu (liuyc@buct.edu.cn) and Weigang Wang (wangwg@iccas.ac.cn)

Abstract:

Nitrous acid (HONO) is an important precursor of OH radicals which affects not only the sinks of primary air pollutants but also the formation of secondary air pollutants, whereas its source closure in the atmosphere is still controversial due to a lack of experiment validation. In this study, the HONO budget in Beijing has been analyzed and validated through the coronavirus disease (COVID-19) lockdown event, which resulted in a significant reduction in air pollutant emissions, providing a rare opportunity to understand the HONO budget in the atmosphere. We measured HONO and related pollutants from January 1, 2020, to March 6, 2020, which covered the Chinese New Year (CNY) and the COVID-19 lockdown. The average concentration of HONO decreased from 0.97 ± 0.74 ppb before CNY to 0.53 ± 0.44 ppb during the COVID-19 lockdown, accompanied by a sharp drop of NO_x and the greatest drop of NO (around 87%). HONO budget analysis suggests that vehicle emissions were the most important source of HONO during the nighttime (53 ± 17%) before CNY, well supported by the decline of their contribution to HONO during the COVID-19 lockdown. We found that the heterogeneous conversion of NO_2 on ground surfaces was an important nighttime source of HONO (31 ± 5%), while that on aerosol surfaces was a minor source (2 ± 1%). Nitrate photolysis became the most important daytime source during the COVID-19 lockdown compared with that before CNY, resulting from the combined effect of the increase in nitrate and the decrease in NO. Our results indicate that reducing vehicle emissions should be an effective measure for alleviating HONO in Beijing.

1. Introduction

As the most vital oxidant in the troposphere, OH radicals not only govern the sink of most trace compounds but also affect the production of secondary pollutants by initiating photochemical reactions in the atmosphere. Nitrous acid (HONO) is an important primary precursor of OH radicals (Kulmala and Petäjä, 2011; Zhang et al., 2023c). Photolysis of HONO can contribute 60% (Tan et al., 2018) and sometimes even 92% (Xue et al., 2020) to OH production in the morning. Therefore, HONO can indirectly promote the formation of both secondary aerosols (Zhang et al., 2019b) and ozone (Zhang et al., 2022a). In addition, HONO can react with histamine to form carcinogens, such as nitrosamines, after entering the human body (Farren et al., 2015). Thus, understanding the sources of HONO in the atmosphere has been a hot topic for several decades, but it is still far from closed (Jiang et al., 2022). Intensive studies have been carried out on HONO measurements and source analysis (Liu et al., 2020c; Liu et al., 2020d; Zheng et al., 2020; Zhang et al., 2020; Xue et al., 2020; Zhang et al., 2019a; Liu et al., 2019b). The concentrations of HONO in the atmosphere range from a few ppt in remote areas (Spataro et al., 2016) to several ppb, even several tens ppb in heavily polluted areas (Liu et al., 2019b; Liu et al., 2020c; Liu et al., 2020d; Zheng et al., 2020).

The sources of atmospheric HONO consist of direct emissions and secondary formation in the atmosphere. Direct emissions include soils, biomass burning, vehicles, indoor air, and livestock farming. Soil emissions, which depend on soil types, microorganisms, water content, temperature, and pH (Kulmala and Petäjä, 2011; Weber et al., 2015; Kim and Or, 2019), are important sources of HONO. Biomass burning, often occurs in the summer and autumn when wheat/corn is harvested and wildfires are common (Zhang et al., 2019b; Sun et al., 2017; Sun

et al., 2018; Peng et al., 2020). Vehicle emissions are considered an important source of HONO in traffic-intensive areas (Kramer et al., 2020; Li et al., 2021). This source is more important at nighttime compared with daytime (Zhang et al., 2016; Fu et al., 2019; Liu et al., 2020d). Recently, indoor emissions have also been proposed as a potential HONO source (Xue, 2022), which is related to the ventilation from high HONO concentrations in indoor air to low HONO concentrations in outdoor air (Zhang et al., 2019b). Livestock farming is a previously overlooked source of HONO, especially in agricultural areas.

Secondary formation of HONO includes gas-phase reaction between NO and OH radicals, photolysis of particulate nitrate, and heterogeneous reaction of NO_2 on ground and particulate matter surfaces, including photochemical heterogeneous reaction of NO_2. Gas phase reaction between NO and OH, photolysis of nitrate particles, and light-enhanced conversion of NO_2 are the main daytime sources of HONO (Liu et al., 2019c; Liu et al., 2020d; Zhang et al., 2022b). Furthermore, acid replacement processes may be a non-negligible source of daytime HONO in locations affected by soil-borne mineral dust deposition (Vandenboer et al., 2014). The heterogeneous reaction of NO_2 on various surfaces is widely regarded as an important source of HONO (Han et al., 2016; Liu et al., 2020b).

Table S1 summarizes the sources of HONO at various locations. The type of observation site often has a great impact on the source intensity and contribution proportion of each source of HONO. In natural ecological areas or Antarctic stations with little human activity, the photolysis of nitrate is the main source of HONO during the day, and its contribution is much higher than the homogeneous reaction of NO and OH (Bond et al., 2023; Tang et al., 2024). In the ocean or areas close to the sea, the heterogeneous transformation of NO_2 becomes the main

source of HONO, and the transformation on the aerosol surface may be more important than that on the ground (Xing et al., 2023). In smoke collected near wildfires, it was found that the heterogeneous conversion contribution of NO_2 can reach 85%, making it the most important source of HONO (Chai et al., 2021). Emissions from soil and biological soil crusts are important in some areas where vegetation and soil are exposed (Meusel et al., 2018). For three different types of observation sites: rural, suburban, and urban, the relative importance of sources is also obviously different. In rural areas, there are usually no traffic activities, and are mainly affected by agricultural activities and animal husbandry, so traffic emissions can be ignored. During periods of intensive agricultural activity, soil emissions are the main source of HONO, accounting for up to 80% (Liu et al., 2019c), When there is little agricultural activity, the reaction of NO and OH and the heterogeneous transformation of NO_2 on the ground become the two main sources in rural areas (Xue et al., 2020; Song et al., 2022), accounting for up to 70%. In rural areas with developed animal husbandry, its direct emissions can contribute 39-45% of HONO (Zhang et al., 2023a). Suburbs are mostly covered by vegetation, with a small number of villages nearby. The heterogeneous conversion of NO_2 is the main source of HONO, which can reach 70% of HONO sources (Fu et al., 2019; Ye et al., 2023). For highways, tunnels, and urban areas with heavy traffic, traffic emissions usually dominate HONO sources, accounting for 40% to 80% of HONO sources (Xu et al., 2015; Zhang et al., 2019c; Liu et al., 2020d; Kramer et al., 2020). In some ordinary urban areas where traffic activities are not so intensive, the heterogeneous conversion of NO_2 and the reaction of NO and OH are also the main sources of HONO in addition to traffic sources. It can be seen that the relative importance of different sources is often affected by the type of emission source near the observation site.

Although intensive studies have been performed on HONO sources, the contributions of different sources are still controversial (Zhou et al., 2011; Liu et al., 2014; Wu et al., 2019; Kramer et al., 2020; Meng et al., 2020). For the same type of observation area, the contribution of each source still diverges in different studies. For example, in mixed residential, commercial, and traffic areas, the importance of traffic emissions varies greatly. In some studies, it accounts for as much as 50% (Liu et al., 2020d; Zhang et al., 2019a; Tong et al., 2016), while in some studies, it can be ignored (Zhang et al., 2020). A similar situation exists for the heterogeneous conversion of NO_2. Some studies suggest that this process is not important (Tong et al., 2015; Zhang et al., 2019c; Zhang et al., 2022b), while some studies believe that it can contribute at least 70% of HONO (Meng et al., 2020; Zhang et al., 2020; Jia et al., 2020). It should be noted that the contribution of NO_2 heterogeneous reaction to HONO greatly depends on the choice of NO_2 uptake coefficient (γ_{NO2}), which varies from 10^{-8} to 10^{-4} in different studies (Meng et al., 2020; Liu et al., 2020b; Ge et al., 2019; Liu et al., 2015; Liu et al., 2020d). Vehicle emissions also have similar characteristics because the HONO emission rate strongly depends on the emission factor, i.e. the ratio of HONO/NO_x (Kramer et al., 2020; R. Kurtenbach et al., 2001; Zhang et al., 2019c), which ranges from 0.03% to 2.1% (Liao et al., 2021). For other HONO sources, the relative importance is affected by many parameters, such as reaction kinetics for photolysis of nitrate, OH concentrations for homogeneous reaction between NO and OH, emission fluxes for soil emissions, and so on. Thus, the HONO budget still has a large uncertainty. In particular, it is an open question how to prove the importance of a specific reaction pathway or a source of atmospheric HONO.

Special events taking place on large spatial scales provide us with an alternative

opportunity to disclose the mysteries of the HONO budget because of obvious and potentially large changes in some of the HONO sources. During the Spring Festival in 2020, the lockdown measures during the new coronavirus disease -19 (COVID-19) pandemic led to a significant reduction in primary emissions from traffic and industries. The magnitude and speed of changes in air pollutant emissions have been considered the largest changes in the history of modern atmospheric chemistry (Kroll et al., 2020). We conducted continuous field observations of HONO and other air pollutants from January 1, 2020, to March 6, 2020, in downtown Beijing, aimed at understanding the changes in HONO concentrations and sources during the lockdown period compared to that before.

2. Experimental section

2.1 Field measurements.

Observations were carried out at the Aerosol and Haze Laboratory, Beijing University of Chemical Technology (AHL/BUCT), which has been described in our previous work (Liu et al., 2020d). Briefly, it is located on the west campus of BUCT, around 550 m from the west third-ring road of Beijing, which is a typical urban observation site. The station is on the rooftop of a 5-story building (about 18 m from the ground). HONO was measured with a homemade Water-based Long-Path Absorption Photometer (LOPAP, Institute of Chemistry, Chinese Academy of Sciences), which has been deployed in field observation studies (Tong et al., 2016; Chen et al., 2020) and has been proven to be a stable and credible instrument for HONO measurements (Crilley et al., 2019). The principle of this instrument is similar to that of a commercial LOPAP (QUMA). Briefly, gas-phase HONO absorbed by deionized water ($\geq$ 18.2 MΩ) in a stripping coil reacts with N-(1-naphthyl) ethylenediamine-dihydrochloric acid (0.077

mmol L^{-1}) in an acidic solution (2 mmol L^{-1} sulfanilamide in 0.12 mol L^{-1} HCl) to form an azo dye, which is measured at 550 nm with a spectrometer equipped with a LWCC (Liquid Waveguide Capillary Cell, LWCC-3250, WPI, USA). The sampling rate was 1 L min^{-1} controlled by a flow meter and a diaphragm pump. The flow rate of absorption liquid was 0.5 ml min^{-1} controlled by a peristaltic pump. The limit of detection of the LOPAP was 0.01 ppb for a sampling duration of 60 s. The instrument was calibrated with nitrite standard solution before and after each measurement about every three weeks and calibrated by zero air every 24 hours to check zero drift. An overestimation of HONO concentration (6.7%), calibrated in control experiments with 100 ppb of NO_2 at 50% RH due to the interference of NO_2 in the sampling inlet (about 30 cm of Teflon tube), was accounted for when we calculating the HONO concentrations in this work.

A set of commercial analyzers for NO_x, SO_2, CO, and O_3 (Thermo Scientific 42i, 43i, 48i, 49i) were also available. Notably, the NO_2 measured by 42i includes HONO, and we have corrected it. $PM_{2.5}$ was measured using a Tapered Element Oscillating Microbalance (TEOM, Thermo Fisher Scientific, 1405). The chemical composition of non-refractory $PM_{2.5}$ (NR-$PM_{2.5}$) was measured using a Time-of-flight Aerosol Chemical Speciation Monitor (ToF-ACSM, Aerodyne). Meteorological parameters including temperature, RH, pressure, wind speed and direction, and ultraviolet radiation (A and B) were measured using a weather station (AWS 310 at AHL/BUCT station, Vaisala). The planetary boundary layer (PBL) height and visibility were measured using a ceilometer (CL51, Vaisala) and a visibility sensor (PWD22, Vaisala), respectively. The photolysis rate (J_{NO2}) was measured via a continuous measurement of the actinic flux in the wavelength range of 285-375 nm using a J_{NO2} filter-radiometer (2-pi-J_{NO2}

183 radiometer, Metcon). All instruments used in the measurement as well as their detection limits
184 are shown in Table S2.

185 **2.2 HONO budget calculation.**

186 Potential sources of HONO include direct emissions (vehicle emissions, soil emissions, indoor
187 emissions, biomass combustion), the gas-phase reaction between NO and OH radicals, the
188 photolysis of nitrate in particulate matter, and the heterogeneous reaction of NO_2 on the ground
189 and particulate matter surfaces. The sources including vehicle emissions ($E_{vehicle}$), soil
190 emissions (E_{soil}), the reaction of NO and OH (P_{NO-OH}), the photolysis of particulate nitrate
191 ($P_{nitrate}$), and the heterogeneous reaction of NO_2 ($P_{aerosol}$ and P_{ground}). At present, there are
192 relatively few studies on indoor emissions. Biomass combustion is an unimportant HONO
193 source in downtown Beijing in winter according to a previous study (Zhang et al., 2019b). Thus,
194 these two sources are not accounted for in this work. The major sinks of HONO, including dry
195 deposition ($L_{deposition}$), the homogeneous reaction with OH radicals ($L_{HONO-OH}$), photolysis
196 ($L_{photolysis}$), and vertical and horizontal transport (T_{trans}), are considered.

197 The calculation method and details in parameterization are shown in Table 1. Briefly, the
198 budget and estimated concentration of HONO can be calculated according to the following
199 equations,

200 $$\frac{dHONO}{dt} = E_{soil} + E_{vehicle} + P_{NO-OH} + P_{nitrate} + P_{aerosol} + P_{ground} -$$

201 $$L_{photolysis} - L_{HONO-OH} - L_{deposition} - T_{trans} \quad (1)$$

202 $$HONO_{est,t_2} = HONO_{obs,t_1} + Sources_{t_2} - Sinks_{t_2} \quad (2)$$

203 where $\frac{dHONO}{dt}$ is the change rate of HONO mixing ratios (ppb h^{-1}), $HONO_{est,t_2}$ is the
204 estimated concentration of HONO at time t_2, while $HONO_{obs,t_1}$ is the observed concentration

of HONO at time t_1. Given that the result of potential source contribution function (PSCF, Fig S2), the source distribution of HONO between BCNY and COVID was highly similar and the trend of HONO was similar (Pearson'r=0.78) between BUCT and Institute of Atmospheric Physics (IAP, 8 km away from BUCT), the steady state analysis on HONO is appliable and reasonable even though the lifetime of HONO is several minutes in the atmosphere. In addition, the instrumentation time resolution of LOPAP was 6 s. We calculated the variation coefficient for the datasets with different time resolutions, i.e., 1 h *vs* 6 s. A small variation coefficient of ~0.02-0.05 implies that a small uncertainty of the HONO budget might result from the lifetime of HONO. Thus, we think the possible uncertainty should not have a large influence on our conclusions when the budget is compared at a fixed site between two different periods. The input parameters for the parameterization scheme are detailed in Table S3 (M0).

The emission rate (E_{HONO}, ppb h^{-1}) of soil and vehicle were calculated based on the emission flux (F_{HONO}, g m^{-2} s^{-1}), the PBL height (H, m), and the conversion factor (α, g m^{-3} s^{-1} to ppb h^{-1}). For vehicle emissions, according to our previous research at the same site, the emission factor (EF, $HONO/NO_x$) was selected as 1.09% (Liu et al., 2020d), which is comparable to the actual values in Hong Kong (1.2 ± 0.4% and 1.24 ± 0.35%) (Liang et al., 2017; Xu et al., 2015), Guangzhou (1.0%) (Li et al., 2012), Beijing (1.3% and 1.41%) (Zhang et al., 2019c; Meng et al., 2020), and other places. For secondary formation, the calculation of the production rate (P_{HONO}, ppb h^{-1}) is shown in Table 1, in which k_1 is the rate constant of the quasi-first order reaction (s^{-1}). For the heterogeneous reaction of NO_2, we calculated the conversion rate in the light of Eqs. (3)-(5):

$$k_{het}^{0} = \frac{HONOcorr,t_2 - HONOcorr,t_1}{\overline{NO_2} \times (t_2 - t_1)} \quad (3)$$

$$k_{het}^{co} = \frac{2\times\left[\frac{HONOcorr,t_2}{CO_{t_2}}\times\overline{CO} - \frac{HONOcorr,t_1}{CO_{t_1}}\times\overline{CO}\right]}{(t_2-t_1)\times\left[\frac{NO_{2,t_2}}{CO_{t_2}}+\frac{NO_{2,t_1}}{CO_{t_1}}\right]\times\overline{CO}}$$

$$= \frac{2\times\left[\frac{HONOcorr,t_2}{CO_{t_2}} - \frac{HONOcorr,t_1}{CO_{t_1}}\right]}{(t_2-t_1)\times\left[\frac{NO_{2,t_2}}{CO_{t_2}}+\frac{NO_{2,t_1}}{CO_{t_1}}\right]} \quad (4)$$

$$k_{het} = \frac{1}{2}\times(k_{het}^{0} + k_{het}^{co}) \quad (5)$$

where k_{het} is the quasi-first-order rate constant of the transformation to HONO (s^{-1}), k_{het}^{0} and k_{het}^{co} are the reaction rate constants after uncalibrated and CO calibrated, respectively (Zhang et al., 2020). To decrease the contribution of boundary layer height variation on the k_{het} calculations, we normalized HONO concentration to CO concentration as the same as reported in the literature (Zhang et al., 2019c; Li et al., 2012). $\overline{NO_2}$ and $\overline{CO}$ are the mean concentration of NO_2 and CO from t_1 to t_2. CO_t and $NO_{2,t}$ are mixing ratios of CO and NO_2, respectively, at the measuring time t. $HONO_{corr,t}$ (ppb) is the HONO concentration corrected after subtracting the primary emissions (including vehicle and soil emissions, and the HONO produced by the homogeneous reaction of NO and OH and the photolysis of nitrate) at the measuring time t according to Eq. (6):

$$HONO_{corr,t} = HONO_t - E_{soil,t} - E_{vehicle,t} - P_{NO-OH,t} - P_{nitrate,t} \quad (6)$$

it is worth noting that the $HONOcorr$ only accounted for vehicle exhausts in previous HONO budget studies. This may overestimate the contribution of heterogeneous reactions to HONO sources because other emission sources and homogeneous reactions should also contribute to HONO.

Meanwhile, when estimating the upper limit of the contribution of heterogeneous reactions, we take a small conversion factor (HONO/NOx) of 0.4% as the lower limit of vehicle emissions, in contrast to the normal value of 1.09% (Liu et al., 2020d). We normalize the

248 EI_{NO_X} caused by the vehicle with the measured NO_X during the observations. This method
249 has also been widely used in previous studies (Liu et al., 2019b; Li et al., 2018). In addition,
250 soil emissions are calculated using the lower limit (Oswald et al., 2013). The mean value of
251 k_{het} during the BCNY (before the Chinese New Year) was 0.0051 h^{-1}, while it was 0.006 h^{-1}
252 in the COVID-19 lockdown, which are consistent with previous studies, such as Ji'nan (0.0068
253 h^{-1}) (Li et al., 2018) and Shanghai (0.007 h^{-1}) (Wang et al., 2013), while less than those in
254 Shijiazhuang (0.016 h^{-1}) (Liu et al., 2020c), Kathmandu (0.014 h^{-1}) (Yu et al., 2009), and
255 Guangzhou (0.016 h^{-1}) (Qin et al., 2009).

256 Table 1. Summary of parameters for HONO sources and sinks

HONO formation/loss pathways	Calculations	Parameters	Reference
Soil emissions → HONO	$E_{HONO} = \alpha \times F_{HONO}/H$	$F_{HONO,soil}$	1
Vehicle emissions → HONO		$F_{HONO,vehicle} = (EI_{NOx,vehicle}/A) \times (HONO/NOx)_{vehicle}$	2
NO + OH → HONO		$k_{NO-OH} = 7.2\times10^{-12}$ cm^3 molecule^{-1} s^{-1}	3
$NO_3^- \xrightarrow{h\nu}$ HONO		$J_{NO3^-} = 8.24\times10^{-5}/3.59\times10^{-7} \times J_{HNO3,MCM}$	
$NO_2 + H_2O \xrightarrow{aerosol\ surface}$ HONO	$P_{HONO} = 3600\times k \times c_{precursor}$	$k_{het} = (\gamma_{NO2} \times A_s \times \omega/4) \times Y_{HONO}$	4
$NO_2 + H_2O \xrightarrow{ground\ surface}$ HONO		$k_{het} = (\gamma_{NO2} \times \delta \times \omega/4H) \times Y_{HONO}$	
HONO $\xrightarrow{h\nu}$ NO + OH	$L_{photolysis} = 3600\times J_{HONO} \times HONO$	$J_{HONO,\ MCM}$	
HONO + OH → H_2O + NO_2	$L_{HONO-OH} = 3600\times k_{HONO-OH} \times HONO \times OH$	$k_{HONO-OH} = 6\times10^{-12}$ cm^3 molecule^{-1} s^{-1}	5
HONO deposition	$L_{deposition} = (3600\times V_d \times HONO)/H$	$V_d = 0.001$m s^{-1}	6
HONO transport (vertical and horizontal)	$T_{trans} = k_{dilution} \times (HONO - HONO_{background})$	$k_{dilution} = 0.23$ h^{-1}	7

$F_{HONO,soil}$ (soil emission flux) was calculated by the temperature-dependent HONO emission flux on grasslands with a water content of 35% to 45%. A is the urban area of Beijing, $EI_{NOx,vehicle}$ is the emission inventory of NO_x from vehicle (g s^{-1}). The calculation of the HONO emission flux, during BCNY, was based on the hourly NO_x emission inventory of Beijing vehicles ($F_{HONO}=F_{NOx} \times (HONO/NOx)_{vehicle}$), while during COVID-19, it was combined with the hourly average traffic index (www.nitrafficindex.com). The $(HONO/NOx)_{vehicle}$ was selected as 1.09% (Liu et al., 2020d). $c_{precursor}$ is the concentration of the precursor (ppb). The OH concentration was estimated using the same method as in the previous study (Liu et al., 2020c). The mean photolysis frequency of nitrate (J_{NO3^-}) was normalized to the measured UV light intensity. A_s is the surface area concentration of the reaction surface (m^2 m^{-3}); ω is the average molecular velocity (m s^{-1}); γ is the uptake coefficient of the precursor, was assumed to be 2×10^{-6}; Y_{HONO} is the yield of HONO. δ is the surface roughness, in this study, we used 3.85 for our calculation (Liu et al., 2020d). *HONO* and $HONO_{background}$ are the HONO concentrations at the observation site and background site, respectively. J_{HONO} is simulated in a box model using J_{NO2} data observed at our site.

1: (Oswald et al., 2013). 2: (Yang et al., 2019). 3: (Liu et al., 2020c). 4: (Liu et al., 2020d). 5: (Kanaya et al., 2007). 6: (Han et al., 2017b). 7: (Dillon et al., 2002).

257

We further derived the uptake coefficient of NO_2 (γ_{NO2}) on both ground and particle surfaces according to Eq. (7).

$$k_{het} = \frac{\gamma_{NO2} \times A_S \times \omega}{4} \times Y_{HONO} \quad (7)$$

The calculated γ_{NO2} ranged from 1×10^{-6} to 3×10^{-6}. Therefore, we choose 2×10^{-6} to calculate the heterogeneous yield of HONO, which is comparable with those derived in urban environments like Ji'nan (1.4×10^{-6}) (Li et al., 2018) and the laboratory experiments (10^{-7} to 10^{-6}) (Han et al., 2013; Stemmler, 2007; Han et al., 2017a) on different particles, but lower than the uptake coefficient of 10^{-5} reported in other studies (Zhang et al., 2020; Ge et al., 2019).

The OH concentration was calculated according to Eq. (8), which is based on the function of the photolysis rates (J) of O_3 and NO_2, and the NO_2 mixing ratio (NO_2).

$$OH = \frac{4.1\times10^{9}\times(J_{NO2})^{0.19}\times(J_{O1D})^{0.83}\times(140NO_2+1)}{0.41NO_2^2+1.7NO_2+1} \quad (8)$$

Notably, this parameterization scheme was developed based on measurements at rural sites (Ehhalt and Rohrer, 2000), where NOx concentrations were lower than in urban environments. Alicke et al. (Alicke, 2002) found that OH concentrations estimated with this scheme were in good agreement with those calculated according to a pseudo-steady state method during the pollution period in urban environments (such as Milan), although some uncertainty was expected. In our previous study (Liu et al., 2020d), we also found that the estimated OH concentrations using this method were comparable with those observed values in the North China Plain (Tan et al., 2019). Thus, daytime OH concentrations estimated using this method should be overall credible although the uncertainty is inevitable. The nocturnal OH concentration in North China generally varied from 1.0×10^5 molecules cm^{-3} (Ma et al., 2019;

Tan et al., 2018) in winter to 5×10^5 molecules cm^{-3} in summer (Tan et al., 2017; Tan et al., 2020). We further parameterized the nocturnal OH concentrations according to atmospheric temperature to reflect the seasonal variations of OH concentration. Fig. S3 summarizes the observed OH concentrations in the North China Plain. The results estimated in this study are slightly lower than those observed in Wangdu (Rural), but almost consistent with those in Beijing (Urban) and Huairou (Suburb). In summary, we should be optimistic about the estimation of OH concentration. Then a sensitivity analysis was performed to understand the influence of the uncertainty of OH concentration on HONO sources as discussed in Section 3.3.

The loss rate of HONO, including dry deposition ($L_{deposition}$), homogeneous reaction with OH radicals ($L_{HONO-OH}$), photolysis ($L_{photolysis}$), and vertical and horizontal transport (T_{trans}), were calculated using the equations shown in Table 1. Where J_{HONO} is the photolysis rate of HONO (s^{-1}), $k_{HONO-OH}$ is the second-order reaction rate constant between HONO and OH, V_d is the dry deposition rate of HONO, and $K_{dilution}$ is the dilution rate (including both vertical and horizontal transport). The details are described in our previous work (Liu et al., 2020c; Liu et al., 2020d).

Oracle Crystal Ball (version 11.1.2.4, Oracle's software for modeling, prediction, simulation, and optimization) (Rahmani et al., 2023) to evaluate the overall uncertainty of the parameterization through Monte Carlo simulations. The details are shown in Text S2 in the SI.

3. Results and discussion

3.1 Air quality during observations.

Figure 1 shows the time series of the concentration and relative proportion of non-refractory components in $PM_{2.5}$, trace gases (SO_2, O_3, CO, NO, NO_2, and NO_x), and meteorological

parameters (temperature, relative humidity (RH), and pressure). We divide the sampling period into two sub-periods, i.e., P1 from January 1 to January 24 (BCNY, before the Chinese New Year) and P2 from January 25 to March 6 (COVID-19 lockdown).

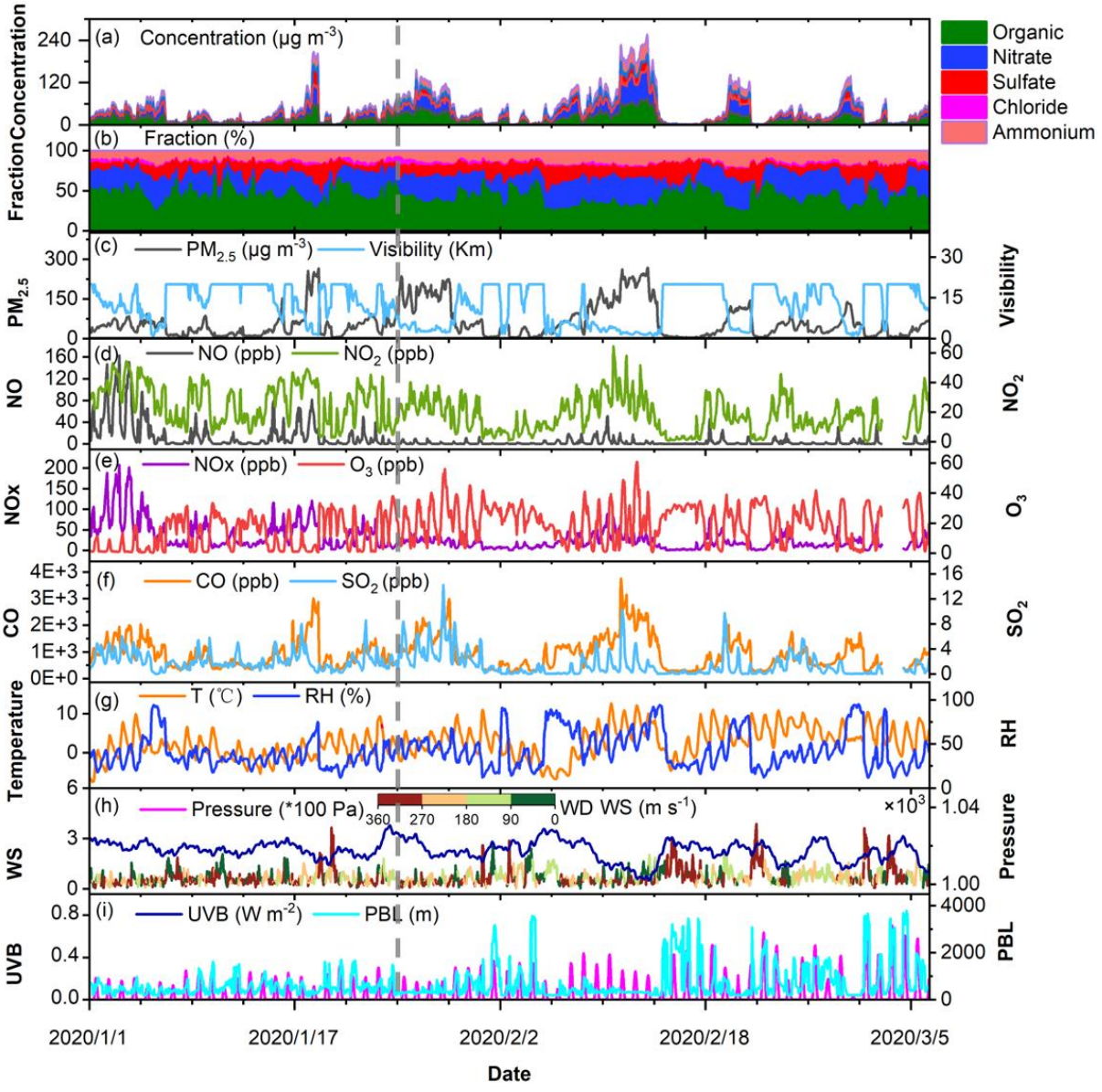

Figure 1. An overview of the measurement of the mass concentrations of the different components of non-refractory-$PM_{2.5}$ (NR-$PM_{2.5}$), the mass fraction of the individual components, $PM_{2.5}$, and meteorological parameters, NO_x (NO, NO_2), O_3, CO and SO_2 in 1-hour average from 1 January to 6 March 2020. Meteorological parameters consist of visibility, PBL heights, UVB, wind speed, wind direction, Pressure, RH, and temperature. The observations

311 are divided into two phases (P1:2020.01.01-2020.01.24 and P2:2020.01.25-2020.03.06).

312

313 It can be seen from Fig. 1 that during P1, there was only one heavy pollution incident
314 lasting one to two days, while there were two serious pollution events lasting more than two
315 days ($PM_{2.5}$ > 75 μg m^{-3}) in the P2 stage. Table S4 summarizes the statistical results of the wind
316 speed, $PM_{2.5}$, RH, T, HONO, trace gases, and NR-$PM_{2.5}$ for the entire measurement period.
317 During P1, the measured concentration of $PM_{2.5}$ varied between 0.2-288 μg m^{-3} and the mean
318 concentration was 47.2 ± 44.5 (mean ± 1σ) μg m^{-3}. In contrast, they were 0.3-258 μg m^{-3} and
319 69.9 ± 67.2 μg m^{-3}, respectively, during P2. The mean concentrations of NO_x decreased
320 significantly ($P < 0.05$) from 45.35 ± 38.86 ppb in P1 to 19.44 ± 14.42 ppb in P2, dropping by
321 about 57%. This is close to the reduction amplitude (50%) reported by Wang et al. (Wang et
322 al., 2020a) but lower than that (76%) proposed by Lv et al (Lv et al., 2020). In particular, the
323 NO mean concentrations dropped from 18.42 ± 29.24 ppb (ranging from 0.03 to 163 ppb) in
324 P1 to 2.4 ± 5.46 ppb (ranging from 0.01 to 51 ppb). The average hourly concentration of NO_2
325 in the P1 phase was 26.9 ± 13.4 ppb, while it was 17.18 ± 11.3 ppb in P2. The NO_2
326 concentration dropped by about 36% from P1 to P2, which is similar to the recently reported
327 findings (ranging from 36% to 53%) (Zhao et al., 2020; Wang et al., 2020b; Wang et al., 2021).
328 According to the emission inventory of NO_x, traffic and industry contributed 46.7% and 31.3%
329 to NO_x emissions in Beijing, respectively (Zheng et al., 2014). This means the decrease in NO_x
330 concentration should be explained by both reductions in traffic and industrial emissions (Lv et
331 al., 2020; Wang et al., 2020a; Zhao et al., 2020). In particular, traffic emissions during P2
332 should play an important role in local NO reduction. However, as the temperature and

ultraviolet light irradiation increased and the NO_x concentration decreased (Kroll et al., 2020; Le et al., 2020), the average concentration of O_3 during P2 was 21.31 ± 11.73 ppb, which was significantly ($P < 0.05$) higher than 12.16 ± 10.79 ppb during P1. This result is similar to the 71.4% increase in O_3 in Shijiazhuang during the same period (Liu et al., 2020c). The concentrations of SO_2 were in the range of 0.02-8.56 ppb with a mean value of 2.09 ± 1.35 ppb in P1, while it varied from 0.01 to 14.23 ppb with the mean concentration of 1.49 ± 1.99 ppb during P2, suggesting slightly decreased contribution of coal combustion during P2 (Fig. 1i). This is similar to that reported by Cui et al (Cui et al., 2020) and Shen et al (Shen et al., 2021). In addition, it can be seen from Fig. 1 that the change trends of $PM_{2.5}$ and CO are synchronized, which also means that both primary emissions and secondary generation contribute to the accumulation of $PM_{2.5}$ concentration (Liu et al., 2020c).

It is worth noting that changes in atmospheric pollutant concentrations are affected by both emissions and meteorology. Especially, during the lockdown period, meteorological conditions in Beijing were not conducive to the dispersion of pollutants, thus the impact of meteorological conditions on the concentration of these pollutants needs to be assessed. We use the random forest algorithm of machine learning to remove the influence of meteorology from air quality time series data by a deweather method. The details are present in Text S1 in the SI. The model performs well in predicting the concentrations of pollutants compared to the observations in both the training and test datasets (Table S5). The concentrations and relative changes of each pollutant after deweather are recorded in Table S6. The $PM_{2.5}$ concentration after deweather increased significantly from 45.22±28.56 in P1 to 67.92±57.97 μg m^{-3} in P2 at a confidence level of 0.05, with an increase of 50.2%. The mean concentration of HONO was

0.89±0.37 ppb in P1, while it decreased to 0.51±0.25 ppb in P2, with a drop of 42.7%; The concentrations of NO and NO_2 significantly decreased from 15.44±18.40 and 23.28±7.28 ppb in P1 to 3.24±2.05 and 16.43±5.98 ppb in P2, respectively, which decreased by 79.0% and 29.4% respectively; SO_2 decreased from 2.27±0.69 in P1 to 1.48±1.18 ppb in P2, a decrease of approximately 34.8%; CO increased from 823.60±318.92 in P1 to 896±488.29 ppb in P2 (an increase of 8.79%) and O_3 increased from 16.98±5.62 to 22.60±4.10 ppb, an increase of about 33.1%, which was much lower than the change range of observed values (75.1%). As shown in Table S6, meteorological conditions have a significant impact on O_3 concentration. The impact was +39.6% and +6.2% in P1 and P2, respectively. The impact of deweather on NO in the two periods was -16.2% and +32.8%, respectively. It was -13.8% and -4.8%, respectively, for NO_2. However, the changes of other species in the two periods after deweather fluctuated between 2.3% and 7.8%. This implies that meteorological conditions have an important impact on the concentrations of NO and O_3, while meteorological factors have little impact on HONO, SO_2, CO, and $PM_{2.5}$.

It can be seen from Figure 1 combined with Table S4 in SI. All the major components of $PM_{2.5}$, including sulfate, nitrate, ammonium, chloride, and organic aerosol, increased obviously in P2 compared to P1. Throughout the entire observation period, organic matter and nitrate dominated the composition of $PM_{2.5}$. The proportion of nitrate in inorganic salts increased to 31.2% in P2, up from 28.1% in P1. Although the sulfate concentration increased, its proportion within inorganic salts slightly decreased on haze days, going from 16.5% in P1 to 15.2% in P2. Thus, the ratio of NO_3^- to SO_4^{2-} during pollution events increased significantly from 1.76 in P1 to 2.10 in P2 ($P < 0.05$). This is similar to previous findings reported by Sun (Sun et al., 2020).

These findings suggest that the decrease in anthropogenic emissions during the P2 period resulted in a significant reduction (After the T-test, it is significant at a confidence level of 0.01.) in gas precursors (Table S4), but it did not lead to a corresponding reduction in secondary aerosol species during periods of pollution. This is supported by the increased potential secondary aerosol formation under pollution conditions (Sun et al., 2020). For example, higher values of the SOR (sulfur oxidation ratio, molar fraction of sulfate in total sulfur including sulfate and SO_2) and NOR (nitrogen oxidation ratio, molar fraction of nitrate in total nitrogen, including nitrate and NO_2), i.e., 0.63 and 0.34, were observed in P2 than those (0.48 and 0.14) in P1. Under stagnant weather conditions (wind speed < 2 m s^{-1}), higher temperatures and RH as shown in Table S4 might facilitate the conversion from precursors into particles (Liu et al., 2020d). The above results indicate that the air pollution dominated by secondary formation is much more serious in P2, which is supported by both the increased concentration and the greater number of pollution days in P2 than in P1, even though primary emissions decreased obviously.

3.2 Influence of Chinese New Year and the COVID-2019 epidemic event on HONO concentration in Beijing.

Figure 2 displays the time series of the HONO concentration, the HONO/NO_2 ratio, and the traffic index (www.nitrafficindex.com). In Fig. 2b, there is a significant decrease in the traffic index ($P < 0.05$), indicating reduced traffic congestion during the COVID-19 lockdown (P2 period) compared to the P1 period. The HONO/NO_2 ratio is frequently used to indicate the conversion of NO_2 to HONO through heterogeneous reactions (Sun et al., 2013). A higher HONO/NO_2 indicates that the heterogeneous conversion process plays a more significant role

in HONO production. However, as depicted in Fig. 2b, both the traffic index and HONO exhibit a similar decreasing trend, while the $HONO/NO_2$ ratio remains relatively stable. Notably, both the traffic index and the NO concentration experienced a steep decline after January 24, coinciding with a significant decrease ($P < 0.05$) in HONO concentration. Furthermore, as shown in Fig. S4, there is a strong correlation between HONO and NO_x in both P1 and P2. However, HONO concentration does not track $PM_{2.5}$ concentration well. These results imply that HONO might be more influenced by vehicle emissions than by heterogeneous reactions on aerosol surfaces. This contrasts with prior studies that heterogeneous reactions on aerosol surfaces are the primary source of HONO in pollution events in Beijing (Liu et al., 2014; Cui et al., 2018; Meng et al., 2020).

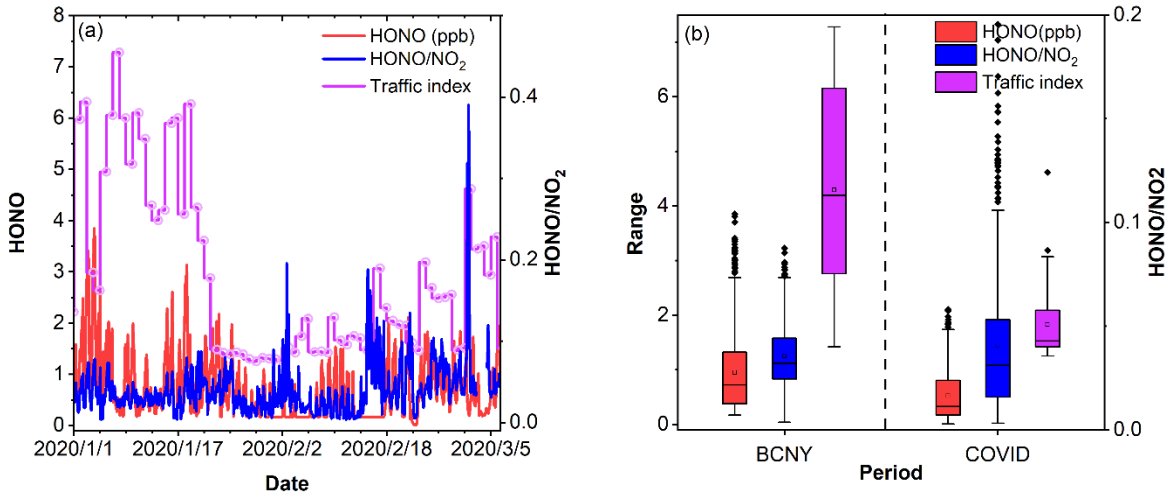

Figure 2. (**a**) Times series of HONO, traffic index, and $HONO/NO_2$, (**b**) Box plots of HONO, $HONO/NO_2$, and the traffic index in Beijing during different periods (BCNY=P1, LOCK=P2).

Table S7 summarizes the mean concentrations of HONO, NO_2, NO, and $PM_{2.5}$ over the two periods in this study as well as the data reported in previous studies. During P1, HONO concentration ranged from 0.17 to 3.85 ppb, with a mean value of 0.97 ± 0.74 ppb. This

concentration is similar to previous observations, such as in Beijing, Xi'an, Jinan, Shanghai, Hong Kong, and Rome, which all ranged from 0.95 to 1.15 ppb (Acker et al., 2006; Wang et al., 2013; Xu et al., 2015; Huang et al., 2017; Liu et al., 2020d; Li et al., 2018). However, during the COVID-19 lockdown, the HONO concentration decreased to 0.53 ± 0.44 ppb, representing a drop of 45.3% compared with that in BCNY. After deweather, the HONO concentration decreased significantly from 0.89±0.37 in P1 to 0.51±0.25 ppb in P2 at a confidence level of 0.05, with a decrease of 42.7%. This means that meteorology has little impact on HONO. This value is comparable to the concentrations reported in the literature for clean days in December 2016 in Beijing (0.5 ± 0.2 ppb) and in the winter of 2018 in Xiamen (0.52-0.61 ppb). At the same time, as discussed in the previous section, the NO concentration decreased by nearly 87% from BCNY to COVID-19 lockdown, and the NO_2 concentration dropped by about 36%. Consequently, we can conclude that the concentrations of HONO, NO, and NO_2 were the most affected pollutants during the COVID-19 lockdown period.

Figure 3 shows the diurnal curves of HONO, NO_x, NO, NO_2, HONO/NO_2, O_3, SO_2, and $PM_{2.5}$×NO_2 during P1 (BCNY) and P2 (COVID-19 lockdown). The black and red lines represent P1 and P2, respectively. HONO shows a similar trend in both periods. After sunset, HONO began to accumulate due to the attenuation of solar radiation and the development of the boundary layer, reaching maximum values of 1.41 ± 0.83 ppb and 0.92 ± 0.64 ppb around 7:00 during P1 and P2, respectively. Subsequently, due to the impact of the boundary layer and rapid photolysis, the HONO concentration gradually decreased and remained at a low level until sunset, with the corresponding minimum value of 0.43 ± 0.24 ppb and 0.27 ± 0.17 ppb at about 15:00. Similar to HONO, the NO_2 concentration shows an upward trend during the

morning rush hour. Its peak appeared at 7:00 (BCNY: 31.4 ± 9.23 ppb; COVID-19 lockdown: 23.3 ± 10.74 ppb), and then dropped rapidly and remained at a low level due to photochemical processes and the development of the boundary layer. The minimum concentration occurs around 14:00 to 15:00 (BCNY: 18.17 ± 10.69 ppb; COVID-19 lockdown: 11.0 ± 7.64 ppb). After sunset, NO_2 began to increase again. It is worth noting that during BCNY, both NO_2 and NO exhibited a prominent evening peak, whereas there was no such evening peak during the COVID-19 lockdown. Thus, NO_x and NO_2 had similar changing trends, i.e., the morning peak observed in both periods with the highest mean values of 65.93 ± 50.37 ppb and 31.7 ± 21.47 ppb in BCNY and COVID-19 lockdown, respectively.

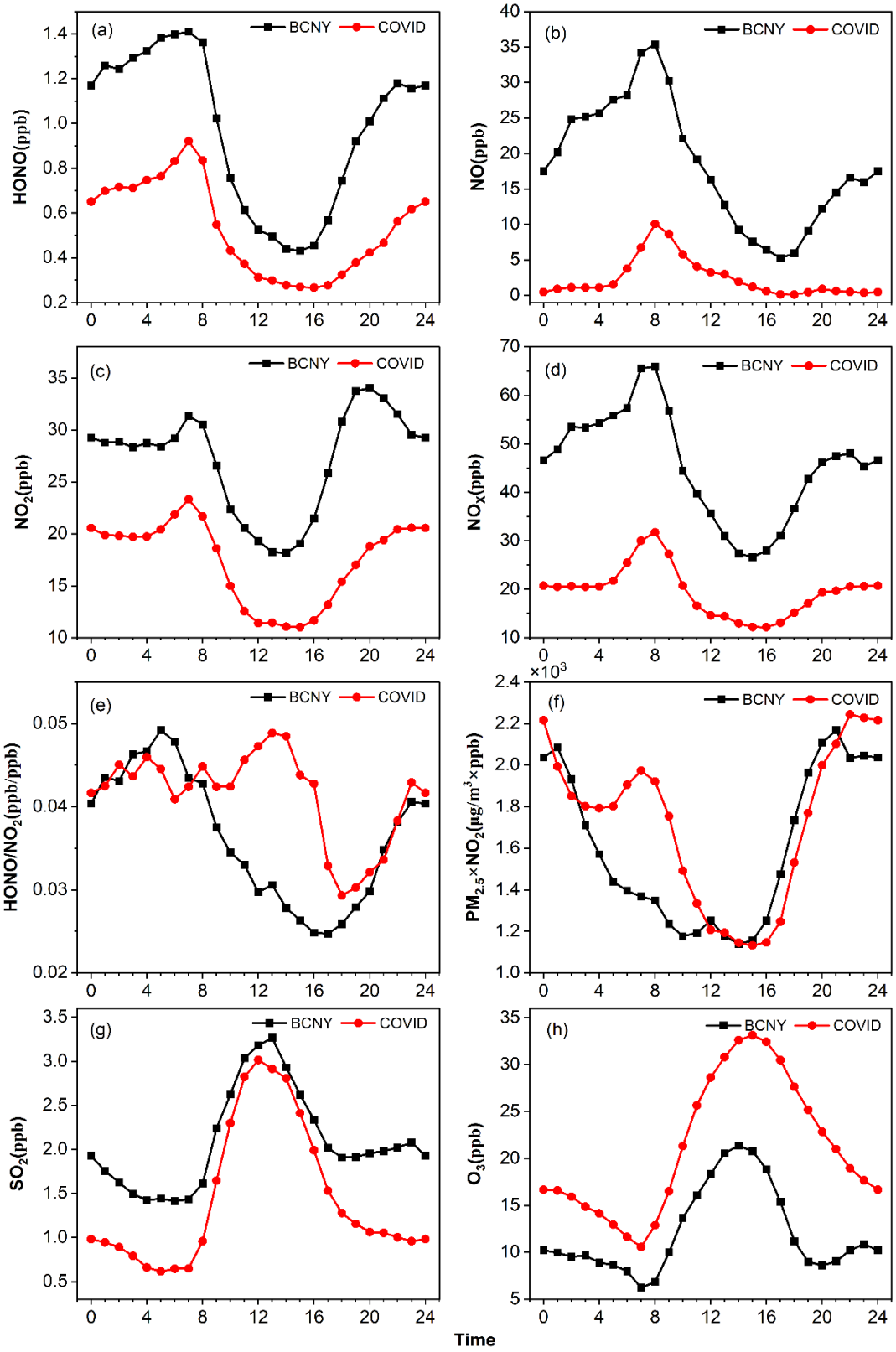

Figure 3. Diurnal variation of HONO, NO, NO_2, NO_x, HONO/NO_2, $PM_{2.5}$×NO_2, SO_2, O_3. The black lines are the diurnal curves before CNY and the red ones are during the COVID-19

lockdown.

NO and HONO showed a similar trend in P1. They began to decline continuously after sunrise and continued to rise after sunset. The peaks of NO were 35.40 ± 43.55 ppb and 10.0 ± 12.67 ppb in P1 and P2, respectively. It is worth noting that the upward trend of NO concentration in the afternoon of the P2 stage was not obvious, as the absolute concentration of NO was very low. O_3 and HONO showed opposite diurnal curves, with the maximum O_3 concentrations occurring in the afternoon, which were 21.35 ± 9.31 ppb and 33.14 ± 10.26 ppb in P1 and P2, respectively. SO_2 and O_3 exhibited similar trends, with the maximum values in P1 and P2 were 3.26 ± 2.19 ppb and 3.01 ± 3.06 ppb at 13:00, and their lowest values were 1.41 ± 0.68 ppb and 0.62 ± 0.82 ppb at 5:00 or 6:00.

Previous studies proposed that the heterogeneous reactions of NO_2 on the aerosol surface play an important role in HONO production. Specifically, this pathway was considered the major source of HONO on polluted days (Cui et al., 2018; Meng et al., 2020; Zhang et al., 2020). $PM_{2.5}\times NO_2$ can be used as an indicator for the heterogeneous reaction of NO_2 on the surface of aerosols (Cui et al., 2018). It was found that the value of $PM_{2.5}\times NO_2$ in P2 (1697 ± 2142) was slightly higher than that in P1 (1583 ± 1967). In the early morning, the product of $PM_{2.5}$ and NO_2 in the P2 stage was even higher than that in the P1 stage. On the other hand, the ratio of HONO/NO_2 is usually used to evaluate the formation of HONO during the conversion of NO_2. As shown in Fig. 3, in the P1 stage, the HONO/NO_2 ratio shows a similar daily trend to HONO, which began to rise after sunset and reached a peak at night and then decreased in the early morning due to the increase of NO_2 concentrations and the photolysis of HONO. In

the P2 stage, the variation of $HONO/NO_2$ is different from that of the P1. The $HONO/NO_2$ in the P2 period was higher than that in the P1 stage, especially in the daytime, although the values of $HONO/NO_2$ in both stages (P1: 0.036 ± 0.016; P2: 0.041 ± 0.038) were lower than that (0.052-0.080) reported by Cui et al (Cui et al., 2018). Subsequently, we further analyzed $HONO_{corr}/NO_2$ (details shown in Sect. 2.2). The $HONO_{corr}/NO_2$ attributed to secondary formation via heterogeneous reactions changed obviously after subtracting other secondary HONO sources. As shown in Fig. S5, the daytime peak of $HONO_{corr}/NO_2$ in P2 became more prominent compared with that in Fig. 3e, while the daytime (8:00 - 18:00) $HONO_{corr}/NO_2$ (0.022 ± 0.014) in P1 was significantly ($P < 0.05$) lower than that in P2 (0.040 ± 0.053). However, the HONO concentration decreased significantly as discussed above. These results suggest that heterogeneous reactions of NO_2 on the aerosol surfaces may not be a major source of HONO because the enhanced potential of heterogeneous reactions indicated by $PM_{2.5}\times NO_2$ and $HONO_{corr}/NO_2$ in P2 contrast with the decreased HONO concentrations compared to P1. In summary, we propose that during our observation period, heterogeneous reactions of NO_2 should have a relatively minor contribution to HONO production.

3.3 Relative change of different sources to HONO budget in Beijing during different periods.

Figure 4a-f shows the diurnal variation of HONO production or emission rates for these sources at different stages, and Fig. 4g-l shows the budget of the HONO sources and sinks during P1 (BCNY) and P2 (COVID-19 lockdown). The HONO production rate via homogeneous reaction between NO and OH in the P1 period was much higher than that in the P2 period, especially during the daytime. The average rate decreased from 0.145 ± 0.189 ppb h^{-1} in the P1

stage to 0.047 ± 0.073 ppb h^{-1} in the P2 stage. The OH concentrations increased slightly from P1 ($4.1\times10^5 \pm 5.8\times10^5$ cm^{-3}) to P2 ($6.7\times10^5 \pm 1.0\times10^6$ cm^{-3}). Therefore, the observed decrease in HONO production rate via homogeneous reaction between NO and OH should be ascribed to the substantial reduction of NO concentration as discussed above. It can be seen that the homogeneous reaction between NO and OH is indeed an important source of HONO at night. In previous studies, the nocturnal production of HONO via NO and OH was often ignored because low nighttime OH concentrations were estimated (Fu et al., 2019). However, some studies have shown that the observed nighttime OH concentrations in the Beijing urban area can also be maintained in the order of 10^5 molecules cm^{-3} in winter, which also means that the contribution of the reaction channels of NO and OH to HONO cannot be ignored. In the P1 stage, the homogeneous reaction between NO and OH accounted for 13 ± 5% of the nighttime HONO sources. However, in the daytime, the homogeneous reaction between NO and OH was the most important source of HONO, which accounted for up to 51 ± 32% of the daytime HONO source. This is consistent with previous studies in urban Beijing (Gu et al., 2021; Jia et al., 2020; Liu et al., 2021). Interestingly, a recent study proposed a new mechanism through smog chamber experiments, that is, NO_x photooxidation (reaction of NO and adsorbed HNO_3) may be an important daytime HONO source (Song et al., 2023), although it has not yet been verified by field observations. In the P2 stage, its proportion in the night was negligible due to the dramatic decrease in NO concentration during the pandemic event, and the maximal proportion of HONO sources in the daytime was also reduced to 25 ± 14%. It is worth noting that the parameterization of OH concentration will introduce uncertainty to HONO sources. Table S3 shows the sensitivity test for the HONO simulation. An increase of 10% and 200% in

OH concentration in M3 and M4 results in a 24-26% change in the HONO source. It means that the accuracy of the OH measurement is important for understanding the source-sink balance of the HONO.

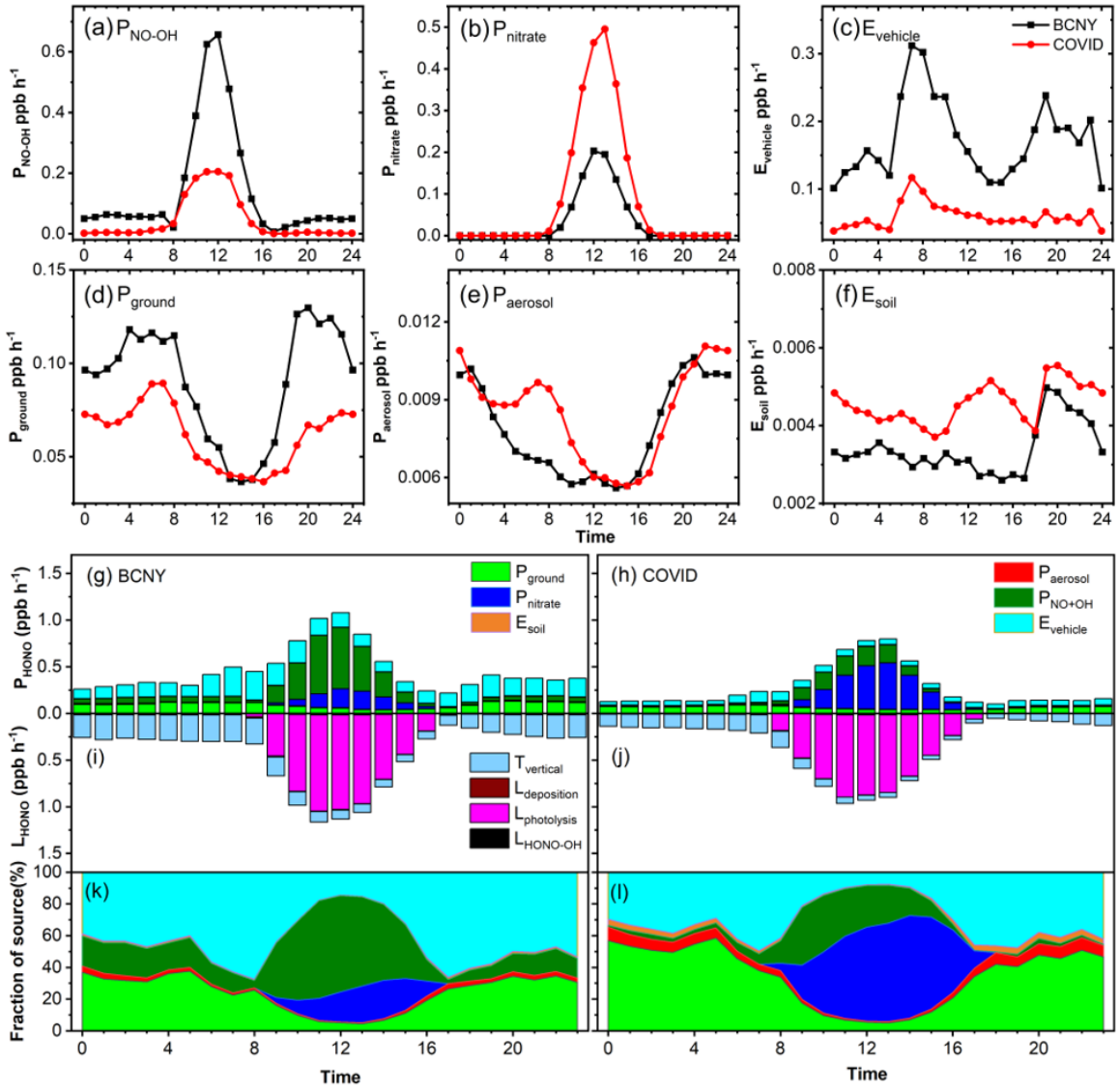

Figure 4. (**a-f**): Diurnal variations in HONO production rate from various sources. The black lines are the diurnal curves before CNY and the red ones are during the COVID-19 lockdown. (**g-l**): Variations of HONO budget. (**g,h**) Diurnal production rates of HONO; (**i,j**) loss rates of HONO (unit: ppb h^{-1}); (**k,l**) relative contributions of each source. Panels (**g**),(**i**), and (**k**) show the data from BCNY, and panels (**h**),(**j**), and (**l**) show the data from the COVID-19 lockdown.

The daytime HONO source related to photolysis of nitrate (0.223 ± 0.175 ppb h^{-1}) in the P2 stage was much larger than that (0.107 ± 0.068 ppb h^{-1}) in the P1 stage. It contributed 16 ± 10% to the daytime HONO source in the P1 period. However, it became the most important daytime source of HONO in the P2 stage, accounting for up to 53 ± 41%, as both the nitrate concentration and the light intensity increased significantly ($P < 0.05$). Ye et al. (Ye et al., 2016) reported that the photolysis rate constants of nitrate particles on the surface of different materials were in the range of 6.0×10^{-6} - 3.7×10^{-4} s^{-1}. Thus, we used the lower limit value of 6.0×10^{-6} s^{-1} and the upper limit value of 3.7×10^{-4} s^{-1} for sensitivity tests (methods M9 and M10), which resulted in a change of 25% and 95% of HONO sources, respectively.

The direct emission rate of HONO from vehicles in the P1 stage was much higher than that in the P2 stage. The emission rate of the P1 stage was between 0.135-0.39 ppb h^{-1}, with a mean value of 0.227 ± 0.071 ppb h^{-1}. This is comparable with the value (0.079-0.32 ppb h^{-1}) in the winter of 2018 (Liu et al., 2020d). In the P2 stage, it decreased to 0.062-0.173 ppb h^{-1}, with a mean value of 0.086 ± 0.027 ppb h^{-1}. This value is slightly higher than the lower limit of vehicle emissions of 0.013-0.076 ppb h^{-1} estimated using an emission factor of 0.18% in our previous study (Liu et al., 2020d), while it is less than the upper limit reported by Li (Li et al., 2018) in Jinan of 0.13 ± 0.06-0.53 ± 0.23 ppb h^{-1}. During the lockdown, the emission rate of HONO from vehicles was reduced by 53%-66% when compared with that before the lockdown. In the P1 period, vehicle emission was an important nighttime source of HONO. It contributed 53 ± 17% to the HONO sources, much higher than heterogeneous reactions of NO_2 on aerosol and ground surfaces (33%) (Fig. S9). In the P2 stage, due to the reduction of transport, the contribution of vehicle emissions to HONO sources decreased to 40 ± 14%, while the

contribution of heterogeneous reactions of NO_2 increased to 53%. This is consistent with the observed decrease in HONO concentrations. The daytime contributions of vehicle emissions to HONO sources were lower than the corresponding nighttime contributions, while it was still higher in the P1 period than in the P2 period. These results mean that vehicles should be important contributors to ambient HONO under typical emission patterns in Beijing. In the sensitivity analysis, the emission factors of 0.008 and 0.0186 were considered in methods M1 and M2, and 8% and 20% changes were found in the simulated HONO sources, respectively. The yield of soil emissions in the P2 stage is also higher than that in the P1 stage due to the temperature rise in the P2 stage because the temperature will affect the soil emission flux (Oswald et al., 2013), while the importance of this source is negligible in this study. In M15 and M16, we amplify and shrink the soil emission flux by 10 times, respectively, and the change of the simulated HONO sources was less than 5%.

As shown in Fig. 4e, the heterogeneous reaction rate of NO_2 on aerosols did not change much between the P1 and P2 stages. The average production rate of HONO in the P1 stage was 0.007 ± 0.002 ppb h^{-1}, and it was 0.008 ± 0.002 ppb h^{-1} in the P2 stage, showing an increase of about 14%. It is worth noting that the HONO formation rate from the heterogeneous conversion of NO_2 on the surface of aerosol does not decrease, which is caused by the increase in $PM_{2.5}$ concentration along with a decrease in NO_2 concentration during the P2 period. If the heterogeneous transformation of NO_2 on particulate surfaces is important, especially in the case of heavy pollution, increased HONO concentrations should be expected instead of a large decrease, as observed in the P2 stage. This is consistent with the changes in $HONO_{corr}/NO_2$ and $PM_{2.5}\times NO_2$ as discussed in Sect. 3.2. For the heterogeneous transformation of NO_2 on the

ground and aerosol surfaces, this source is sensitive to the uptake coefficient (γ) of NO_2. For the aerosol surface, here we assume that the upper limit of γ is 10^{-5} (M7) and the lower limit is 2×10^{-7} (M8) (Liu et al., 2019b; Liu et al., 2020d). As shown in Table S3, the change in simulated HONO is less than 5%. We reduced and magnified the surface area concentration (A_s) of particulate matter by a factor of 10 in M11 and M12, respectively, and the resulting change in HONO was still less than 10%. It should be noted that HONO is sensitive to the uptake coefficient and surface area concentration. When the uptake coefficient is expanded by 5 times or reduced by 10 times, the absolute HONO flux attributed to heterogeneous reactions increases 5 times or decreases 10 times, while the relative contribution is very low due to the small absolute value of heterogeneous reactions compared with other sources.

Regarding the heterogeneous reaction of NO_2 on ground surfaces, the average formation rate of HONO in the P1 stage was 0.09 ± 0.03 ppb h^{-1}, while it was 0.06 ± 0.02 ppb h^{-1} in the P2 stage. This is ascribed to the significant drop ($P < 0.05$) in NO_2 concentration during the COVID-19 lockdown. Fig. 4k shows that the heterogeneous reaction of NO_2 on ground surfaces is also an important nighttime source of HONO. In the P1 stage, heterogeneous reactions on both aerosol and ground surfaces explained 33% of the nighttime HONO source. In the daytime, however, the contribution of heterogeneous reactions to HONO sources dropped rapidly. In the P2 stage, the heterogeneous reaction became the most important nighttime source contributing up to 53% of HONO (Fig. S9). This can be explained by the significant decrease ($P < 0.05$) in NO and direct emissions of HONO from traffic. Similar to heterogeneous reactions on aerosol surfaces, we assumed that the upper limit of γ_{NO2} on ground surfaces was 10^{-5} (M5) and the lower limit was 2×10^{-7} (M6), respectively, and the

changes in simulated HONO source were 40% and 9%, respectively. Indicating that HONO is sensitive to the NO_2 uptake coefficient on the ground surface. In M13 and M14, we set the surface roughness (δ) to 1 and 2.2 as reported in the literature, respectively (Zhang et al., 2022b; Liu et al., 2020c), and the simulated changes in HONO were less than 8%.

During the P1 and P2 periods, the mean values of $T_{vertical}$ were 0.195 ± 0.076 ppb h^{-1} and 0.102 ± 0.048 ppb h^{-1}, respectively. It was the main sink of HONO at night. The mean $L_{photolysis}$ was 0.563 ± 0.375 ppb h^{-1} and 0.442 ± 0.324 ppb h^{-1}, respectively, which was the main daytime sink of HONO. The average loss rate of $L_{HONO\text{-}OH}$ during P1 and P2 was 0.005 ppb h^{-1} and 0.004 ppb h^{-1}, respectively. The $L_{deposition}$ was 0.009 ± 0.005 ppb h^{-1} during P1, while it was 0.004 ± 0.003 ppb h^{-1} during P2. In M17 and M18, we set the lower limit of the deposition rate (V_d) to 0.00077 and the upper limit to 0.025 (Zhang et al., 2023b), causing a change of 1% and 24% in the simulated HONO, respectively. In M19 and M20 at the same time, we set the dilution rate ($K_{dilution}$) to 0.1 and 0.44, resulting in a 12% and 19% change, respectively.

It should be noted that each source is sensitive to the corresponding parameter as discussed above. Thus, a more restrictive criterion is required to evaluate the reasonability of the parameterization. We further estimated the HONO concentration according to Eq. (2) and the parameters described in Sect. 2.2 to verify these calculated sources and sinks of HONO. Fig. S6 shows the time series of estimated HONO concentrations. The observed HONO concentrations were also shown for comparison. The estimated HONO concentrations were well correlated with the observed values from the perspective of both diurnal curves and the scattering point plot during the whole period (Fig. S7 and Fig. S8) although the estimated HONO concentrations were slightly lower than the observed values at noon as shown in Fig.

S7. This means that our parametric scheme is overall reasonable but still underestimates the daytime HONO source due to some unknown daytime sources. This unknown source may be related to the photochemical reactions related to NO_2 and nitroaromatic compounds mentioned in recent studies (Liu et al., 2020a). Liu et al. have found the photoenhanced effect of the conversion from NO_2 to HONO on real urban grime and glass windows simulated in laboratory studies (Liu et al., 2019a; Liu et al., 2020b). Yang et al. also have proposed that photolysis of nitroaromatic compounds may be a daytime source of HONO (Yang et al., 2021). Considering the uncertainty of parameterization, we used Oracle Crystal Ball (version 11.1.2.4, Oracle's software for modeling, prediction, simulation, and optimization) (Rahmani et al., 2023) to evaluate the overall uncertainty of the parameterization through Monte Carlo simulations. The relative standard deviation is 27.2% for the HONO budget (details are in SI).

In summary, heterogeneous reactions of NO_2 (including ground and aerosol surfaces) contributed 33% to the nocturnal HONO sources in the P1 stage, while they increased to 53% in the P2 stage. Ground surfaces were the main interfaces for heterogeneous reactions, compared to aerosol surfaces. At the same time, vehicle emissions account for 53 ± 17% and 40 ± 14% of nighttime HONO sources in the P1 and P2 stages, respectively. To explore whether meteorological factors have an impact on the sources of HONO, we conducted the budget analysis of HONO using the deweathered pollutant concentrations. The results are shown in Fig. S10. When compared with the sources of HONO calculated using the raw concentration dataset (Fig. S9), it can be seen that deweathering has little effect on the daytime sources of HONO. For the nighttime source of HONO, however, deweathering caused the proportion of traffic emissions during BCNY increasing from 53% to 63% before the CNY or from 40% to

635 45% during the COVID-19 lockdown. The contribution of heterogeneous reactions of NO_2 on
636 ground surfaces decreased from 31% to 19% before the CNY or from 47% to 42% during the
637 COVID-19 lockdown. These results further highlight the importance of vehicle emissions to
638 nocturnal HONO sources in Beijing.

639 Therefore, regardless of whether the impact of meteorological conditions on the source of
640 HONO is considered, we can conclude that traffic-related emissions, rather than heterogeneous
641 reactions of NO_2 were the main HONO source at night in Beijing in the typical emission
642 patterns of air pollutants.

643 **4. Conclusions and atmospheric implications**.

644 During the COVID-19 pandemic at the beginning of 2020, the concentration of many air
645 pollutants decreased significantly ($P < 0.05$) due to the emission reduction of factories and
646 transportation. The average concentration of NO_x decreased by about 57%, of which NO
647 decreased by about 87%, and NO_2 decreased by about 36%. The average concentration of
648 HONO decreased by about 45.3% compared with those before the pandemic control. The
649 average concentration of O_3 and $PM_{2.5}$ increased by approximately 75% and 50%, respectively.
650 It is worth noting that in addition to primary emissions, meteorological changes will also affect
651 changes in atmospheric pollutant concentrations. After removing meteorological factors, the
652 change proportions of $PM_{2.5}$ concentration in the two stages were -4.3% and -2.3% respectively.
653 The HONO changes were -8.3% and -3.8% respectively, the CO changes were -9.3% and -6.2%
654 respectively, and the SO_2 changes were +8.6% and +0.7% respectively. The change proportions
655 are all less than 10%, which means that the impact of changes in meteorological factors on
656 $PM_{2.5}$, HONO, CO, and SO_2 is very weak. However, the change proportions of NO in the two

stages were -16.2% and +32.8%, respectively, and O_3 was +39.6% and +6.2% respectively. The change ratio is greater than 30%, indicating that NO and O_3 are greatly affected by meteorology. In addition, the changes in NO_2 were -13.8% and -4.8% respectively, implying that NO_2 is also affected by meteorological factors. From the entire observation period, except for O_3, the changes of other species in the two periods fluctuated between 2.3% and 7.8% after deweather, all less than 8%. In general, after removing the meteorological effects, NO increased by 79%, NO_2 increased by approximately 29%, HONO decreased by approximately 43%, and $PM_{2.5}$ increased by approximately 50%. It is worth noting that O_3 increased by about 33%, which is much lower than the change in observed values (75.1%) (as shown in Table S6). Although we have tried to assess the impact of meteorological factors quantitatively, this still carries some uncertainty. In particular, uncertainty is inevitable for the source assessment of substances such as HONO that are affected by a large number of parameters.

In this study, the parameters of HONO sources were optimized. The balance of sources and sinks is well supported by a relatively high correlation between observed and estimated HONO concentrations. During the observation period, we used lockdown during COVID-19 as a disturbance factor and compared the concentration and source changes of HONO before and during COVID-19 lockdown to determine whether heterogeneous reactions on the surface of particulate matter and vehicle emissions were important HONO sources. We found that vehicle-related emissions were the most important nighttime HONO source in Beijing, contributing 50-60% to the nighttime HONO sources. The homogeneous reaction between NO and OH and the heterogeneous reaction of NO_2 on the aerosol surface were not important for the contribution of nocturnal HONO, accounting for 13 ± 5% and 2 ± 1%, respectively. The

heterogeneous reaction of NO_2 on ground surfaces was also found to be an important source of HONO at night, accounting for 31 ± 5% of the nighttime HONO sources. Nitrate photolysis became the most important source of HONO during the daytime compared with the situation before the pandemic control because of the combined effect of the increase in the average concentration of nitrate and the decrease in the NO concentration during the pandemic. We conducted a potential source contribution function (PSCF, Fig S2) analysis in different periods, i.e., BCNY and COVID, at the BUCT station and further compared the PSCF of HONO at BUCT station with that at the Institute Atmospheric Physics (IAP) station, which is around 8 km from BUCT station, from January 24, 2022, to January 31, 2022, when the data were available. The PSCF patterns were highly similar in different periods or locations. These results mean that the air mass should be consistent during the COVID-19 lockdown and BCNY and HONO should be evenly distributed in Beijing. Thus, the impact of meteorological changes on the accuracy of observations cannot be ruled out, which is also a limitation of this study, but its influence should be comparable between BCNY and the COVID lockdown. And the conclusions drawn based on the observations at BUCT should represent the situation in Beijing. Through uncertainty assessment, it was found that the assumption of $J_{NO_3^-}$ would have the greatest uncertainty, with a standard deviation of ±19%. Nevertheless, this study confirms that reducing anthropogenic emissions can indeed reduce the concentration of HONO in the atmosphere. However, such reduction does not have a simple linear relation with the reduction in human activities, but it also depends on meteorological conditions and complex chemical transformation processes taking place in the atmosphere.

As a megacity in China, Beijing has a large population and intensive traffic emissions, as

a result of frequent air pollution. Although concentrations of HONO are usually lower than those of other major pollutants, HONO efficiently triggers the formation of secondary pollutants acting as an important primary source of OH radicals. Therefore, the sources of HONO deserve to be investigated for air pollution control in Beijing. Our results suggest that motor vehicle emissions are an important HONO source, while the contribution of the heterogeneous conversion of NO_2 to HONO on the aerosol surfaces still needs to be further evaluated and, especially, the kinetic parameters on ambient aerosol should be determined. In future research, it is necessary to combine field observations, laboratory studies, and model simulations to quantify the contribution of traffic-related emissions to HONO, and finally obtain an accurate budget of HONO.

Author contributions: YZ contributed to the methodology, data curation, and writing of the original draft. ZF and FZ contributed to the methodology, investigation, and data curation. CL contributed to methodology, investigation, and data curation. WW contributed to the conceptualization, investigation, reviewing, and editing the text, and supervision. XF contributed to the methodology, reviewing, and editing the text. YZ and WM contributed to the methodology, investigation, data curation, and reviewing and editing the text. ZL and CL contributed to methodology, investigation, and data curation. GZ contributed to the methodology, investigation, resources, and data curation. CY contributed to the methodology, data curation, reviewing, and editing the text. VK, FB, TP, and JK contributed to the acquisition of resources and reviewing and editing the text. MK contributed to the methodology and reviewed the text. YL contributed to the conceptualization, investigation, data curation, writing, reviewing & editing, supervision, and funding acquisition;

Competing interests: At least one of the (co-)authors is a member of the editorial board of Atmospheric Chemistry and Physics.

Data availability: Data are available upon request to Yongchun Liu (liuyc@buct.edu.cn).

Acknowledgments: This research was financially supported by the Beijing Natural Science Foundation (8232041), Beijing National Laboratory for Molecular Sciences (BNLMS-CXXM-202011), and the National Natural Science Foundation of China (42275117 and 41931287). This research was supported in part by Hebei Technological Innovation Center for Volatile Organic Compounds Detection and Treatment in Chemical Industry (ZXJJ20220406) and the Natural Science Foundation of Hebei Province (D2023209012). The work is partially supported by Academy of Finland Flagship "Atmosphere and Climate Competence Center

(ACCC), project number 337549 and European Union's Horizon 2020 research and innovation programme under grant agreement No 101036245 (RI-URBANS) and 101056783 (FOCI) as well as Technology Industries of Finland Centennial Foundation via project "urbaani ilmanlaatu 2.0". The authors would like to thank Dr. Zirui Liu from the Institute of Atmospheric Physics, Chinese Academy of Sciences, for providing HONO dataset for comparison.

References

Acker, K., Febo, A., Trick, S., Perrino, C., Bruno, P., Wiesen, P., Möller, D., Wieprecht, W., Auel, R., Giusto, M., Geyer, A., Platt, U., and Allegrini, I.: Nitrous acid in the urban area of Rome, Atmospheric Environment, 40, 3123-3133, 10.1016/j.atmosenv.2006.01.028, 2006.

Alicke, B.: Impact of nitrous acid photolysis on the total hydroxyl radical budget during the Limitation of Oxidant Production/Pianura Padana Produzione di Ozono study in Milan, Journal of Geophysical Research, 107, 10.1029/2000jd000075, 2002.

Bond, A. M. H., Frey, M. M., Kaiser, J., Kleffmann, J., Jones, A. E., and Squires, F. A.: Snowpack nitrate photolysis drives the summertime atmospheric nitrous acid (HONO) budget in coastal Antarctica, Atmospheric Chemistry and Physics, 23, 5533-5550, 10.5194/acp-23-5533-2023, 2023.

Chai, J., Dibb, J. E., Anderson, B. E., Bekker, C., Blum, D. E., Heim, E., Jordan, C. E., Joyce, E. E., Kaspari, J. H., Munro, H., Walters, W. W., and Hastings, M. G.: Isotopic evidence for dominant secondary production of HONO in near-ground wildfire plumes, Atmospheric Chemistry and Physics, 21, 13077-13098, 10.5194/acp-21-13077-2021, 2021.

Chen, Y., Wang, W., Lian, C., Peng, C., Zhang, W., Li, J., Liu, M., Shi, B., Wang, X., and Ge, M.: Evaluation and impact factors of indoor and outdoor gas-phase nitrous acid under different environmental conditions, J Environ Sci (China), 95, 165-171, 10.1016/j.jes.2020.03.048, 2020.

Crilley, L. R., Kramer, L. J., Ouyang, B., Duan, J., Zhang, W., Tong, S., Ge, M., Tang, K., Qin, M., Xie, P., Shaw, M. D., Lewis, A. C., Mehra, A., Bannan, T. J., Worrall, S. D., Priestley, M., Bacak, A., Coe, H., Allan, J., Percival, C. J., Popoola, O. A. M., Jones, R. L., and Bloss, W. J.: Intercomparison of nitrous acid (HONO) measurement techniques in a megacity (Beijing), Atmos. Meas. Tech., 12, 6449-6463, 10.5194/amt-12-6449-2019, 2019.

Cui, L., Li, R., Zhang, Y., Meng, Y., Fu, H., and Chen, J.: An observational study of nitrous acid (HONO) in Shanghai, China: The aerosol impact on HONO formation during the haze episodes, Sci Total Environ, 630, 1057-1070, 10.1016/j.scitotenv.2018.02.063, 2018.

Cui, Y., Ji, D., Maenhaut, W., Gao, W., Zhang, R., and Wang, Y.: Levels and sources of hourly PM2.5-related elements during the control period of the COVID-19 pandemic at a rural site between Beijing and Tianjin, Sci Total Environ, 744, 140840, 10.1016/j.scitotenv.2020.140840, 2020.

Dillon, M. B., Lamanna, M. S., Schade, G. W., Goldstein, A. H., and Cohen, R. C.: Chemical evolution of the Sacramento urban plume: Transport and oxidation, Journal of Geophysical Research: Atmospheres, 107, ACH 3-1-ACH 3-15, 10.1029/2001jd000969, 2002.

Ehhalt, D. H. and Rohrer, F.: Dependence of the OH concentration on solar UV, Journal of Geophysical Research: Atmospheres, 105, 3565-3571, 10.1029/1999jd901070, 2000.

Farren, N. J., Ramirez, N., Lee, J. D., Finessi, E., Lewis, A. C., and Hamilton, J. F.: Estimated Exposure Risks from Carcinogenic Nitrosamines in Urban Airborne Particulate Matter, Environ Sci Technol, 49, 9648-9656, 10.1021/acs.est.5b01620, 2015.

Fu, X., Wang, T., Zhang, L., Li, Q., Wang, Z., Xia, M., Yun, H., Wang, W., Yu, C., Yue, D., Zhou, Y., Zheng, J., and Han, R.: The significant contribution of HONO to secondary pollutants during a severe winter pollution event in southern China, Atmospheric Chemistry and Physics, 19, 1-14, 10.5194/acp-19-1-2019, 2019.

Ge, S., Wang, G., Zhang, S., Li, D., Xie, Y., Wu, C., Yuan, Q., Chen, J., and Zhang, H.: Abundant NH3 in China Enhances Atmospheric HONO Production by Promoting the Heterogeneous Reaction of SO2 with NO2, Environ Sci Technol, 53, 14339-14347, 10.1021/acs.est.9b04196, 2019.

Gu, R., Shen, H., Xue, L., Wang, T., Gao, J., Li, H., Liang, Y., Xia, M., Yu, C., Liu, Y., and Wang, W.: Investigating the sources of atmospheric nitrous acid (HONO) in the megacity of Beijing, China, Science of The Total

Environment, 10.1016/j.scitotenv.2021.152270, 2021.
Han, C., Liu, Y., and He, H.: Role of organic carbon in heterogeneous reaction of NO2 with soot, Environ Sci Technol, 47, 3174-3181, 10.1021/es304468n, 2013.
Han, C., Liu, Y., and He, H.: Heterogeneous reaction of NO2 with soot at different relative humidity, Environ Sci Pollut Res Int, 24, 21248-21255, 10.1007/s11356-017-9766-y, 2017a.
Han, C., Yang, W., Wu, Q., Yang, H., and Xue, X.: Heterogeneous Photochemical Conversion of NO2 to HONO on the Humic Acid Surface under Simulated Sunlight, Environ Sci Technol, 50, 5017-5023, 10.1021/acs.est.5b05101, 2016.
Han, X., Zhang, M., Skorokhod, A., and Kou, X.: Modeling dry deposition of reactive nitrogen in China with RAMS-CMAQ, Atmospheric Environment, 166, 47-61, 10.1016/j.atmosenv.2017.07.015, 2017b.
Hao, Q., Jiang, N., Zhang, R., Yang, L., and Li, S.: Characteristics, sources and reactions of nitrous acid during winter in the core city of the Central Plains Economic Region in China via high-time-resolution online, Atmospheric Chemistry and Physics Discussions, 10.5194/acp-2019-916, 2019.
Huang, R. J., Yang, L., Cao, J., Wang, Q., Tie, X., Ho, K. F., Shen, Z., Zhang, R., Li, G., Zhu, C., Zhang, N., Dai, W., Zhou, J., Liu, S., Chen, Y., Chen, J., and O'Dowd, C. D.: Concentration and sources of atmospheric nitrous acid (HONO) at an urban site in Western China, Sci Total Environ, 593-594, 165-172, 10.1016/j.scitotenv.2017.02.166, 2017.
Jia, C., Tong, S., Zhang, W., Zhang, X., Li, W., Wang, Z., Wang, L., Liu, Z., Hu, B., Zhao, P., and Ge, M.: Pollution characteristics and potential sources of nitrous acid (HONO) in early autumn 2018 of Beijing, Sci Total Environ, 735, 139317, 10.1016/j.scitotenv.2020.139317, 2020.
Jiang, Y., Xue, L., Shen, H., Dong, C., Xiao, Z., and Wang, W.: Dominant Processes of HONO Derived from Multiple Field Observations in Contrasting Environments, Environmental Science & Technology Letters, 9, 258-264, 10.1021/acs.estlett.2c00004, 2022.
Kanaya, Y., Cao, R., Akimoto, H., Fukuda, M., Komazaki, Y., Yokouchi, Y., Koike, M., Tanimoto, H., Takegawa, N., and Kondo, Y.: Urban photochemistry in central Tokyo: 1. Observed and modeled OH and HO2radical concentrations during the winter and summer of 2004, Journal of Geophysical Research, 112, 10.1029/2007jd008670, 2007.
Kim, M. and Or, D.: Microscale pH variations during drying of soils and desert biocrusts affect HONO and NH3 emissions, Nat Commun, 10, 3944, 10.1038/s41467-019-11956-6, 2019.
Kramer, L. J., Crilley, L. R., Adams, T. J., Ball, S. M., Pope, F. D., and Bloss, W. J.: Nitrous acid (HONO) emissions under real-world driving conditions from vehicles in a UK road tunnel, Atmospheric Chemistry and Physics, 20, 5231-5248, 10.5194/acp-20-5231-2020, 2020.
Kroll, J. H., Heald, C. L., Cappa, C. D., Farmer, D. K., Fry, J. L., Murphy, J. G., and Steiner, A. L.: The complex chemical effects of COVID-19 shutdowns on air quality, Nat Chem, 12, 777-779, 10.1038/s41557-020-0535-z, 2020.
Kulmala, M. and Petäjä, T.: Soil Nitrites Influence Atmospheric Chemistry, Science 333, 1586-1587, 2011.
Le, T., Wang, Y., Liu, L., Yang, J., Yung, Y. L., Li, G., and Seinfeld, J. H.: Unexpected air pollution with marked emission reductions during the COVID-19 outbreak in China, Science, 369, 702-+, 10.1126/science.abb7431, 2020.
Li, D., Xue, L., Wen, L., Wang, X., Chen, T., Mellouki, A., Chen, J., and Wang, W.: Characteristics and sources of nitrous acid in an urban atmosphere of northern China: Results from 1-yr continuous observations, Atmospheric Environment, 182, 296-306, 10.1016/j.atmosenv.2018.03.033, 2018.
Li, S., Song, W., Zhan, H., Zhang, Y., Zhang, X., Li, W., Tong, S., Pei, C., Wang, Y., Chen, Y., Huang, Z., Zhang, R., Zhu, M., Fang, H., Wu, Z., Wang, J., Luo, S., Fu, X., Xiao, S., Huang, X., Zeng, J., Zhang, H., Chen, D.,

826 Gligorovski, S., Ge, M., George, C., and Wang, X.: Contribution of Vehicle Emission and NO2 Surface
827 Conversion to Nitrous Acid (HONO) in Urban Environments: Implications from Tests in a Tunnel, Environ Sci
828 Technol, 10.1021/acs.est.1c00405, 2021.
829 Li, X., Brauers, T., Häseler, R., Bohn, B., Fuchs, H., Hofzumahaus, A., Holland, F., Lou, S., Lu, K. D., Rohrer, F.,
830 Hu, M., Zeng, L. M., Zhang, Y. H., Garland, R. M., Su, H., Nowak, A., Wiedensohler, A., Takegawa, N., Shao,
831 M., and Wahner, A.: Exploring the atmospheric chemistry of nitrous acid (HONO) at a rural site in Southern China,
832 Atmospheric Chemistry and Physics, 12, 1497-1513, 10.5194/acp-12-1497-2012, 2012.
833 Liang, Y., Zha, Q., Wang, W., Cui, L., Lui, K. H., Ho, K. F., Wang, Z., Lee, S. C., and Wang, T.: Revisiting nitrous
834 acid (HONO) emission from on-road vehicles: A tunnel study with a mixed fleet, J Air Waste Manag Assoc, 67,
835 797-805, 10.1080/10962247.2017.1293573, 2017.
836 Liao, S., Zhang, J., Yu, F., Zhu, M., Liu, J., Ou, J., Dong, H., Sha, Q., Zhong, Z., Xie, Y., Luo, H., Zhang, L., and
837 Zheng, J.: High Gaseous Nitrous Acid (HONO) Emissions from Light-Duty Diesel Vehicles, Environ Sci Technol,
838 55, 200-208, 10.1021/acs.est.0c05599, 2021.
839 Liu, J., Deng, H., Lakey, P. S. J., Jiang, H., Mekic, M., Wang, X., Shiraiwa, M., and Gligorovski, S.: Unexpectedly
840 High Indoor HONO Concentrations Associated with Photochemical NO2 Transformation on Glass Windows,
841 Environmental Science & Technology, 54, 15680-15688, 10.1021/acs.est.0c05624, 2020a.
842 Liu, J., Li, S., Mekic, M., Jiang, H., Zhou, W., Loisel, G., Song, W., Wang, X., and Gligorovski, S.: Photoenhanced
843 Uptake of NO2 and HONO Formation on Real Urban Grime, Environmental Science & Technology Letters, 6,
844 413-417, 10.1021/acs.estlett.9b00308, 2019a.
845 Liu, J., Deng, H., Li, S., Jiang, H., Mekic, M., Zhou, W., Wang, Y., Loisel, G., Wang, X., and Gligorovski, S.:
846 Light-enhanced heterogeneous conversion of NO2 to HONO on solid films consisted of fluorene and
847 fluorene/Na2SO4: An impact on urban and indoor atmosphere, Environ Sci Technol, 10.1021/acs.est.0c02627,
848 2020b.
849 Liu, J., Liu, Z., Ma, Z., Yang, S., Yao, D., Zhao, S., Hu, B., Tang, G., Sun, J., Cheng, M., Xu, Z., and Wang, Y.:
850 Detailed budget analysis of HONO in Beijing, China: Implication on atmosphere oxidation capacity in polluted
851 megacity, Atmospheric Environment, 244, 10.1016/j.atmosenv.2020.117957, 2021.
852 Liu, Y., Han, C., Ma, J., Bao, X., and He, H.: Influence of relative humidity on heterogeneous kinetics of NO2 on
853 kaolin and hematite, Phys Chem Chem Phys, 17, 19424-19431, 10.1039/c5cp02223a, 2015.
854 Liu, Y., Nie, W., Xu, Z., Wang, T., Wang, R., Li, Y., Wang, L., Chi, X., and Ding, A.: Semi-quantitative
855 understanding of source contribution to nitrous acid (HONO) based on 1 year of continuous observation at the
856 SORPES station in eastern China, Atmospheric Chemistry and Physics, 19, 13289-13308, 10.5194/acp-19-13289-
857 2019, 2019b.
858 Liu, Y., Ni, S., Jiang, T., Xing, S., Zhang, Y., Bao, X., Feng, Z., Fan, X., Zhang, L., and Feng, H.: Influence of
859 Chinese New Year overlapping COVID-19 lockdown on HONO sources in Shijiazhuang, Sci Total Environ, 745,
860 141025, 10.1016/j.scitotenv.2020.141025, 2020c.
861 Liu, Y., Lu, K., Li, X., Dong, H., Tan, Z., Wang, H., Zou, Q., Wu, Y., Zeng, L., Hu, M., Min, K. E., Kecorius, S.,
862 Wiedensohler, A., and Zhang, Y.: A Comprehensive Model Test of the HONO Sources Constrained to Field
863 Measurements at Rural North China Plain, Environ Sci Technol, 53, 3517-3525, 10.1021/acs.est.8b06367, 2019c.
864 Liu, Y., Zhang, Y., Lian, C., Yan, C., Feng, Z., Zheng, F., Fan, X., Chen, Y., Wang, W., Chu, B., Wang, Y., Cai, J.,
865 Du, W., Daellenbach, K. R., Kangasluoma, J., Bianchi, F., Kujansuu, J., Petäjä, T., Wang, X., Hu, B., Wang, Y.,
866 Ge, M., He, H., and Kulmala, M.: The promotion effect of nitrous acid on aerosol formation in wintertime in
867 Beijing: the possible contribution of traffic-related emissions, Atmospheric Chemistry and Physics, 20, 13023-
868 13040, 10.5194/acp-20-13023-2020, 2020d.
869 Liu, Z., Wang, Y., Costabile, F., Amoroso, A., Zhao, C., Huey, L. G., Stickel, R., Liao, J., and Zhu, T.: Evidence

of aerosols as a media for rapid daytime HONO production over China, Environ Sci Technol, 48, 14386-14391, 10.1021/es504163z, 2014.
Lv, Z., Wang, X., Deng, F., Ying, Q., Archibald, A. T., Jones, R. L., Ding, Y., Cheng, Y., Fu, M., Liu, Y., Man, H., Xue, Z., He, K., Hao, J., and Liu, H.: Source-Receptor Relationship Revealed by the Halted Traffic and Aggravated Haze in Beijing during the COVID-19 Lockdown, Environ Sci Technol, 54, 15660-15670, 10.1021/acs.est.0c04941, 2020.
Ma, X., Tan, Z., Lu, K., Yang, X., Liu, Y., Li, S., Li, X., Chen, S., Novelli, A., Cho, C., Zeng, L., Wahner, A., and Zhang, Y.: Winter photochemistry in Beijing: Observation and model simulation of OH and HO2 radicals at an urban site, Sci Total Environ, 685, 85-95, 10.1016/j.scitotenv.2019.05.329, 2019.
Meng, F., Qin, M., Tang, K., Duan, J., Fang, W., Liang, S., Ye, K., Xie, P., Sun, Y., Xie, C., Ye, C., Fu, P., Liu, J., and Liu, W.: High-resolution vertical distribution and sources of HONO and NO2 in the nocturnal boundary layer in urban Beijing, China, Atmospheric Chemistry and Physics, 20, 5071-5092, 10.5194/acp-20-5071-2020, 2020.
Meusel, H., Tamm, A., Kuhn, U., Wu, D., Leifke, A. L., Fiedler, S., Ruckteschler, N., Yordanova, P., Lang-Yona, N., Pöhlker, M., Lelieveld, J., Hoffmann, T., Pöschl, U., Su, H., Weber, B., and Cheng, Y.: Emission of nitrous acid from soil and biological soil crusts represents an important source of HONO in the remote atmosphere in Cyprus, Atmospheric Chemistry and Physics, 18, 799-813, 10.5194/acp-18-799-2018, 2018.
Nie, W., Ding, A. J., Xie, Y. N., Xu, Z., Mao, H., Kerminen, V. M., Zheng, L. F., Qi, X. M., Huang, X., Yang, X. Q., Sun, J. N., Herrmann, E., Petäjä, T., Kulmala, M., and Fu, C. B.: Influence of biomass burning plumes on HONO chemistry in eastern China, Atmospheric Chemistry and Physics, 15, 1147-1159, 10.5194/acp-15-1147-2015, 2015.
Oswald, R., Behrendt, T., Ermel, M., Wu, D., Su, H., Cheng, Y., Breuninger, C., Moravek, A., Mougin, E., Delon, C., Loubet, B., Pommerening-Roser, A., Sorgel, M., Poschl, U., Hoffmann, T., Andreae, M. O., Meixner, F. X., and Trebs, I.: HONO emissions from soil bacteria as a major source of atmospheric reactive nitrogen, Science, 341, 1233-1235, 10.1126/science.1242266, 2013.
Peng, Q., Palm, B. B., Melander, K. E., Lee, B. H., Hall, S. R., Ullmann, K., Campos, T., Weinheimer, A. J., Apel, E. C., Hornbrook, R. S., Hills, A. J., Montzka, D. D., Flocke, F., Hu, L., Permar, W., Wielgasz, C., Lindaas, J., Pollack, I. B., Fischer, E. V., Bertram, T. H., and Thornton, J. A.: HONO Emissions from Western U.S. Wildfires Provide Dominant Radical Source in Fresh Wildfire Smoke, Environ Sci Technol, 54, 5954-5963, 10.1021/acs.est.0c00126, 2020.
Pusede, S. E., VandenBoer, T. C., Murphy, J. G., Markovic, M. Z., Young, C. J., Veres, P. R., Roberts, J. M., Washenfelder, R. A., Brown, S. S., Ren, X., Tsai, C., Stutz, J., Brune, W. H., Browne, E. C., Wooldridge, P. J., Graham, A. R., Weber, R., Goldstein, A. H., Dusanter, S., Griffith, S. M., Stevens, P. S., Lefer, B. L., and Cohen, R. C.: An Atmospheric Constraint on the NO2 Dependence of Daytime Near-Surface Nitrous Acid (HONO), Environ Sci Technol, 49, 12774-12781, 10.1021/acs.est.5b02511, 2015.
Qin, M., Xie, P., Su, H., Gu, J., Peng, F., Li, S., Zeng, L., Liu, J., Liu, W., and Zhang, Y.: An observational study of the HONO–NO2 coupling at an urban site in Guangzhou City, South China, Atmospheric Environment, 43, 5731-5742, 10.1016/j.atmosenv.2009.08.017, 2009.
R. Kurtenbach, K.H. Becker, J.A.G. Gomes, J. Kleffmann, J.C. L.orzer, M. Spittler, P. Wiesen, R. Ackermann, A. Geyer, and Platt, U.: Investigations of emissions and heterogeneous formation of HONO in a road traffic tunnel, Atmospheric Environment, , 3385–3394, 2001.
Rahmani, A., Khamutian, S., Doosti-Irani, A., Saatchi, O., and Shokoohizadeh, M. J.: Arsenic level in drinking water, its correlation with water quality parameters, and associated health risks, Environmental Monitoring and Assessment, 195, 10.1007/s10661-023-11486-1, 2023.
Shen, N., Zhao, X., Li, L., Zhou, B., Duan, F., and Zhao, W.: Spatial and temporal variation characteristics of

914 atmospheric NO2 and SO2 in the Beijing-Tianjin-Hebei region before and after the COVID-19 outbreak, Air Qual
915 Atmos Health, 1-14, 10.1007/s11869-021-01016-8, 2021.
916 Song, M., Zhao, X., Liu, P., Mu, J., He, G., Zhang, C., Tong, S., Xue, C., Zhao, X., Ge, M., and Mu, Y.:
917 Atmospheric NOx oxidation as major sources for nitrous acid (HONO), npj Climate and Atmospheric Science, 6,
918 10.1038/s41612-023-00357-8, 2023.
919 Song, Y., Zhang, Y., Xue, C., Liu, P., He, X., Li, X., and Mu, Y.: The seasonal variations and potential sources of
920 nitrous acid (HONO) in the rural North China Plain, Environ Pollut, 311, 119967, 10.1016/j.envpol.2022.119967,
921 2022.
922 Spataro, F., Ianniello, A., Salvatori, R., Nardino, M., Esposito, G., and Montagnoli, M.: Sources of atmospheric
923 nitrous acid (HONO) in the European High Arctic, Rendiconti Lincei, 28, 25-33, 10.1007/s12210-016-0568-9,
924 2016.
925 Stemmler, K.: Light induced conversion of nitrogen dioxide into nitrous acid on submicron humic acid aerosol,
926 Atmospheric Chemistry and Physics, 2007.
927 Sun, J., Shen, Z., Zeng, Y., Niu, X., Wang, J., Cao, J., Gong, X., Xu, H., Wang, T., Liu, H., and Yang, L.:
928 Characterization and cytotoxicity of PAHs in PM2.5 emitted from residential solid fuel burning in the Guanzhong
929 Plain, China, Environ Pollut, 241, 359-368, 10.1016/j.envpol.2018.05.076, 2018.
930 Sun, J., Shen, Z., Cao, J., Zhang, L., Wu, T., Zhang, Q., Yin, X., Lei, Y., Huang, Y., Huang, R. J., Liu, S., Han, Y.,
931 Xu, H., Zheng, C., and Liu, P.: Particulate matters emitted from maize straw burning for winter heating in rural
932 areas in Guanzhong Plain, China: Current emission and future reduction, Atmospheric Research, 184, 66-76,
933 10.1016/j.atmosres.2016.10.006, 2017.
934 Sun, Y., Lei, L., Zhou, W., Chen, C., He, Y., Sun, J., Li, Z., Xu, W., Wang, Q., Ji, D., Fu, P., Wang, Z., and Worsnop,
935 D. R.: A chemical cocktail during the COVID-19 outbreak in Beijing, China: Insights from six-year aerosol
936 particle composition measurements during the Chinese New Year holiday, Sci Total Environ, 742, 140739,
937 10.1016/j.scitotenv.2020.140739, 2020.
938 Sun, Y. L., Wang, Z. F., Fu, P. Q., Yang, T., Jiang, Q., Dong, H. B., Li, J., and Jia, J. J.: Aerosol composition,
939 sources and processes during wintertime in Beijing, China, Atmospheric Chemistry and Physics, 13, 4577-4592,
940 10.5194/acp-13-4577-2013, 2013.
941 Tan, Z., Lu, K., Jiang, M., Su, R., Wang, H., Lou, S., Fu, Q., Zhai, C., Tan, Q., Yue, D., Chen, D., Wang, Z., Xie,
942 S., Zeng, L., and Zhang, Y.: Daytime atmospheric oxidation capacity in four Chinese megacities during the
943 photochemically polluted season: a case study based on box model simulation, Atmospheric Chemistry and
944 Physics, 19, 3493-3513, 10.5194/acp-19-3493-2019, 2019.
945 Tan, Z., Hofzumahaus, A., Lu, K., Brown, S. S., Holland, F., Huey, L. G., Kiendler-Scharr, A., Li, X., Liu, X., Ma,
946 N., Min, K. E., Rohrer, F., Shao, M., Wahner, A., Wang, Y., Wiedensohler, A., Wu, Y., Wu, Z., Zeng, L., Zhang,
947 Y., and Fuchs, H.: No Evidence for a Significant Impact of Heterogeneous Chemistry on Radical Concentrations
948 in the North China Plain in Summer 2014, Environ Sci Technol, 54, 5973-5979, 10.1021/acs.est.0c00525, 2020.
949 Tan, Z., Fuchs, H., Lu, K., Hofzumahaus, A., Bohn, B., Broch, S., Dong, H., Gomm, S., Häseler, R., He, L.,
950 Holland, F., Li, X., Liu, Y., Lu, S., Rohrer, F., Shao, M., Wang, B., Wang, M., Wu, Y., Zeng, L., Zhang, Y., Wahner,
951 A., and Zhang, Y.: Radical chemistry at a rural site (Wangdu) in the North China Plain: observation and model
952 calculations of OH, HO2 and RO2 radicals, Atmospheric Chemistry and Physics, 17, 663-690, 10.5194/acp-17-
953 663-2017, 2017.
954 Tan, Z., Rohrer, F., Lu, K., Ma, X., Bohn, B., Broch, S., Dong, H., Fuchs, H., Gkatzelis, G. I., Hofzumahaus, A.,
955 Holland, F., Li, X., Liu, Y., Liu, Y., Novelli, A., Shao, M., Wang, H., Wu, Y., Zeng, L., Hu, M., Kiendler-Scharr,
956 A., Wahner, A., and Zhang, Y.: Wintertime photochemistry in Beijing: observations of ROx radical concentrations
957 in the North China Plain during the BEST-ONE campaign, Atmospheric Chemistry and Physics, 18, 12391-12411,

10.5194/acp-18-12391-2018, 2018.
Tang, M.-X., He, L.-Y., Xia, S.-Y., Jiang, Z., He, D.-Y., Guo, S., Hu, R.-Z., Zeng, H., and Huang, X.-F.: Coarse particles compensate for missing daytime sources of nitrous acid and enhance atmospheric oxidation capacity in a coastal atmosphere, Science of The Total Environment, 915, 10.1016/j.scitotenv.2024.170037, 2024.
Tong, S., Hou, S., Zhang, Y., Chu, B., Liu, Y., He, H., Zhao, P., and Ge, M.: Comparisons of measured nitrous acid (HONO) concentrations in a pollution period at urban and suburban Beijing, in autumn of 2014, Science China Chemistry, 58, 1393-1402, 10.1007/s11426-015-5454-2, 2015.
Tong, S., Hou, S., Zhang, Y., Chu, B., Liu, Y., He, H., Zhao, P., and Ge, M.: Exploring the nitrous acid (HONO) formation mechanism in winter Beijing: direct emissions and heterogeneous production in urban and suburban areas, Faraday Discuss, 189, 213-230, 10.1039/c5fd00163c, 2016.
VandenBoer, T. C., Young, C. J., Talukdar, R. K., Markovic, M. Z., Brown, S. S., Roberts, J. M., and Murphy, J. G.: Nocturnal loss and daytime source of nitrous acid through reactive uptake and displacement, Nature Geoscience, 8, 55-60, 10.1038/ngeo2298, 2014.
Wang, J., Xu, X., Wang, S., He, S., Li, X., and He, P.: Heterogeneous effects of COVID-19 lockdown measures on air quality in Northern China, Appl Energy, 282, 116179, 10.1016/j.apenergy.2020.116179, 2021.
Wang, P., Chen, K., Zhu, S., Wang, P., and Zhang, H.: Severe air pollution events not avoided by reduced anthropogenic activities during COVID-19 outbreak, Resour Conserv Recycl, 158, 104814, 10.1016/j.resconrec.2020.104814, 2020a.
Wang, S., Zhou, R., Zhao, H., Wang, Z., Chen, L., and Zhou, B.: Long-term observation of atmospheric nitrous acid (HONO) and its implication to local NO2 levels in Shanghai, China, Atmospheric Environment, 77, 718-724, 10.1016/j.atmosenv.2013.05.071, 2013.
Wang, Y., Wen, Y., Wang, Y., Zhang, S., Zhang, K. M., Zheng, H., Xing, J., Wu, Y., and Hao, J.: Four-Month Changes in Air Quality during and after the COVID-19 Lockdown in Six Megacities in China, Environmental Science & Technology Letters, 7, 802-808, 10.1021/acs.estlett.0c00605, 2020b.
Weber, B., Wu, D., Tamm, A., Ruckteschler, N., Rodriguez-Caballero, E., Steinkamp, J., Meusel, H., Elbert, W., Behrendt, T., Sorgel, M., Cheng, Y., Crutzen, P. J., Su, H., and Poschl, U.: Biological soil crusts accelerate the nitrogen cycle through large NO and HONO emissions in drylands, Proc Natl Acad Sci U S A, 112, 15384-15389, 10.1073/pnas.1515818112, 2015.
Wu, D., Horn, M. A., Behrendt, T., Muller, S., Li, J., Cole, J. A., Xie, B., Ju, X., Li, G., Ermel, M., Oswald, R., Frohlich-Nowoisky, J., Hoor, P., Hu, C., Liu, M., Andreae, M. O., Poschl, U., Cheng, Y., Su, H., Trebs, I., Weber, B., and Sorgel, M.: Soil HONO emissions at high moisture content are driven by microbial nitrate reduction to nitrite: tackling the HONO puzzle, ISME J, 13, 1688-1699, 10.1038/s41396-019-0379-y, 2019.
Xing, C., Xu, S., Song, Y., Liu, C., Liu, Y., Lu, K., Tan, W., Zhang, C., Hu, Q., Wang, S., Wu, H., and Lin, H.: A new insight into the vertical differences in NO2 heterogeneous reaction to produce HONO over inland and marginal seas, Atmospheric Chemistry and Physics, 23, 5815-5834, 10.5194/acp-23-5815-2023, 2023.
Xu, Z., Wang, T., Wu, J., Xue, L., Chan, J., Zha, Q., Zhou, S., Louie, P. K. K., and Luk, C. W. Y.: Nitrous acid (HONO) in a polluted subtropical atmosphere: Seasonal variability, direct vehicle emissions and heterogeneous production at ground surface, Atmospheric Environment, 106, 100-109, 10.1016/j.atmosenv.2015.01.061, 2015.
Xue, C.: Substantially Growing Interest in the Chemistry of Nitrous Acid (HONO) in China: Current Achievements, Problems, and Future Directions, Environ Sci Technol, 10.1021/acs.est.2c02237, 2022.
Xue, C., Zhang, C., Ye, C., Liu, P., Catoire, V., Krysztofiak, G., Chen, H., Ren, Y., Zhao, X., Wang, J., Zhang, F., Zhang, C., Zhang, J., An, J., Wang, T., Chen, J., Kleffmann, J., Mellouki, A., and Mu, Y.: HONO Budget and Its Role in Nitrate Formation in the Rural North China Plain, Environmental Science & Technology, 54, 11048-11057, 10.1021/acs.est.0c01832, 2020.

Yang, D., Zhang, S., Niu, T., Wang, Y., Xu, H., Zhang, K. M., and Wu, Y.: High-resolution mapping of vehicle emissions of atmospheric pollutants based on large-scale, real-world traffic datasets, Atmospheric Chemistry and Physics, 19, 8831-8843, 10.5194/acp-19-8831-2019, 2019.
Yang, W., You, D., Li, C., Han, C., Tang, N., Yang, H., and Xue, X.: Photolysis of Nitroaromatic Compounds under Sunlight: A Possible Daytime Photochemical Source of Nitrous Acid?, Environmental Science & Technology Letters, 8, 747-752, 10.1021/acs.estlett.1c00614, 2021.
Ye, C., Gao, H., Zhang, N., and Zhou, X.: Photolysis of Nitric Acid and Nitrate on Natural and Artificial Surfaces, Environ Sci Technol, 50, 3530-3536, 10.1021/acs.est.5b05032, 2016.
Ye, C., Lu, K., Ma, X., Qiu, W., Li, S., Yang, X., Xue, C., Zhai, T., Liu, Y., Li, X., Li, Y., Wang, H., Tan, Z., Chen, X., Dong, H., Zeng, L., Hu, M., and Zhang, Y.: HONO chemistry at a suburban site during the EXPLORE-YRD campaign in 2018: formation mechanisms and impacts on O3 production, Atmospheric Chemistry and Physics, 23, 15455-15472, 10.5194/acp-23-15455-2023, 2023.
Yu, Y., Galle, B., Panday, A., Hodson, E., Prinn, R., and Wang, S.: Observations of high rates of NO2-HONO conversion in the nocturnal atmospheric boundary layer in Kathmandu, Nepal, Atmospheric Chemistry and Physics, 6401–6415, 2009.
Zhang, J., An, J., Qu, Y., Liu, X., and Chen, Y.: Impacts of potential HONO sources on the concentrations of oxidants and secondary organic aerosols in the Beijing-Tianjin-Hebei region of China, Sci Total Environ, 647, 836-852, 10.1016/j.scitotenv.2018.08.030, 2019a.
Zhang, J., Chen, J., Xue, C., Chen, H., Zhang, Q., Liu, X., Mu, Y., Guo, Y., Wang, D., Chen, Y., Li, J., Qu, Y., and An, J.: Impacts of six potential HONO sources on HOx budgets and SOA formation during a wintertime heavy haze period in the North China Plain, Sci Total Environ, 681, 110-123, 10.1016/j.scitotenv.2019.05.100, 2019b.
Zhang, J., Lian, C., Wang, W., Ge, M., Guo, Y., Ran, H., Zhang, Y., Zheng, F., Fan, X., Yan, C., Daellenbach, K. R., Liu, Y., Kulmala, M., and An, J.: Amplified role of potential HONO sources in O3 formation in North China Plain during autumn haze aggravating processes, Atmospheric Chemistry and Physics, 22, 3275-3302, 10.5194/acp-22-3275-2022, 2022a.
Zhang, L., Wang, T., Zhang, Q., Zheng, J., Xu, Z., and Lv, M.: Potential sources of nitrous acid (HONO) and their impacts on ozone: A WRF-Chem study in a polluted subtropical region, Journal of Geophysical Research: Atmospheres, 121, 3645-3662, 10.1002/2015jd024468, 2016.
Zhang, Q., Liu, P., George, C., Chen, T., Ren, Y., Mu, Y., Song, M., Herrmann, H., Mellouki, A., Chen, J., Zhao, X., and Zeng, Y.: Unveiling the underestimated direct emissions of nitrous acid (HONO), Proceedings of the National Academy of Sciences, 120, 10.1073/pnas, 2023a.
Zhang, W., Tong, S., Ge, M., An, J., Shi, Z., Hou, S., Xia, K., Qu, Y., Zhang, H., Chu, B., Sun, Y., and He, H.: Variations and sources of nitrous acid (HONO) during a severe pollution episode in Beijing in winter 2016, Sci Total Environ, 648, 253-262, 10.1016/j.scitotenv.2018.08.133, 2019c.
Zhang, W., Ren, Y., Zhang, C., Liu, P., Xue, C., Ye, C., Liu, C., Wang, J., Zhang, Y., Liu, J., Song, Y., Feng, Y., and Mu, Y.: Aging of pollution air parcels acts as the dominant source for nocturnal HONO, Sci Total Environ, 881, 163438, 10.1016/j.scitotenv.2023.163438, 2023b.
Zhang, W., Tong, S., Jia, C., Wang, L., Liu, B., Tang, G., Ji, D., Hu, B., Liu, Z., Li, W., Wang, Z., Liu, Y., Wang, Y., and Ge, M.: Different HONO Sources for Three Layers at the Urban Area of Beijing, Environ Sci Technol, 54, 12870-12880, 10.1021/acs.est.0c02146, 2020.
Zhang, X., Tong, S., Jia, C., Zhang, W., Wang, Z., Tang, G., Hu, B., Liu, Z., Wang, L., Zhao, P., Pan, Y., and Ge, M.: Elucidating HONO formation mechanism and its essential contribution to OH during haze events, npj Climate and Atmospheric Science, 6, 10.1038/s41612-023-00371-w, 2023c.
Zhang, X., Tong, S., Jia, C., Zhang, W., Li, J., Wang, W., Sun, Y., Wang, X., Wang, L., Ji, D., Wang, L., Zhao, P.,

Tang, G., Xin, J., Li, A., and Ge, M.: The Levels and Sources of Nitrous Acid (HONO) in Winter of Beijing and Sanmenxia, Journal of Geophysical Research: Atmospheres, 127, 10.1029/2021jd036278, 2022b.

Zhao, Y., Zhang, K., Xu, X., Shen, H., Zhu, X., Zhang, Y., Hu, Y., and Shen, G.: Substantial Changes in Nitrogen Dioxide and Ozone after Excluding Meteorological Impacts during the COVID-19 Outbreak in Mainland China, Environmental Science & Technology Letters, 7, 402-408, 10.1021/acs.estlett.0c00304, 2020.

Zheng, B., Huo, H., Zhang, Q., Yao, Z. L., Wang, X. T., Yang, X. F., Liu, H., and He, K. B.: High-resolution mapping of vehicle emissions in China in 2008, Atmospheric Chemistry and Physics, 14, 9787-9805, 10.5194/acp-14-9787-2014, 2014.

Zheng, J., Shi, X., Ma, Y., Ren, X., Jabbour, H., Diao, Y., Wang, W., Ge, Y., Zhang, Y., and Zhu, W.: Contribution of nitrous acid to the atmospheric oxidation capacity in an industrial zone in the Yangtze River Delta region of China, Atmospheric Chemistry and Physics, 20, 5457-5475, 10.5194/acp-20-5457-2020, 2020.

Zhou, X., Zhang, N., TerAvest, M., Tang, D., Hou, J., Bertman, S., Alaghmand, M., Shepson, P. B., Carroll, M. A., Griffith, S., Dusanter, S., and Stevens, P. S.: Nitric acid photolysis on forest canopy surface as a source for tropospheric nitrous acid, Nature Geoscience, 4, 440-443, 10.1038/ngeo1164, 2011.